REPAIRS TO DAMAGE TOLERANT AIRCRAFT

by

T. SWIFT

FEDERAL AVIATION ADMINISTRATION

presented to

INTERNATIONAL SYMPOSIUM ON STRUCTURAL INTEGRITY OF AGING AIRPLANES

ATLANTA, GEORGIA

20 - 22 MARCH, 1990

REPAIRS TO DAMAGE TOLERANT AIRCRAFT

T. SWIFT

Federal Aviation Administration
3229 E Spring Street
Long Beach, Calif. 90806-2425

Summary

The results of displacement compatibility analysis, representing a variety of repair doubler and lap splice configurations, are presented with a view to illustrating how structural repairs can degrade the fatigue initiation life and damage tolerance capability of primary transport aircraft structure. Examples show that fatigue initiation life is directly related to the peak loads induced in the first fastener rows at the edges of repair doublers. Design of repairs to an equal or better static strength capability and the associated static strength analysis will not normally highlight these peak loads which can result in considerable degradation of structural fatigue life. Critical fastener loads, based on displacement compatibility analysis accounting for fastener flexibility, are parametrically presented for a variety of skin and doubler thicknesses. Suggestions are made on how repair designs can be modified to improve fatigue initiation life and subsequent fatigue crack detectability particularly in the event of multiple-site damage (MSD). The importance of riveting quality during repairs, often not up to initial manufacturing standards, is discussed with respect to fatigue initiation life. A simplified but conservative method to generate crack growth curves is discussed with a view to easing the analytical burden for the small modifiers. It is hoped that this information, together with conservative fatigue Sn data, will help the many small repair and modification stations gain an appreciation of the fatigue and damage tolerance quality of structural repairs. It is pointed out in the paper that the FAA regulations were amended in December, 1978 for new transport category aircraft and in May, 1981 for aging transport aircraft to include a damage tolerance philosophy. This means that any repair to a transport category airframe, which may effect threshold, frequency and type of inspection of principal structural elements, must be evaluated for it's damage tolerance capability.

Introduction

In December, 1978 the Federal Aviation Administration amended their Fatigue Evaluation requirements for Transport Category Airplanes to include a damage tolerance philosophy. Prior to this time FAR 25.571, Fatigue Evaluation of Flight Structure, included an option to design to either "Fail-Safe" or "Safe-Life" principles. The manufacturers had generally adopted the Fail-Safe option with the exception of a few components such as

engine mounts and landing gear. In satisfying the regulation to the Fail-Safe option they had designed structure to be redundant so that catastrophic failure would not result after fatigue failure or obvious partial failure of a single principal structural element. However, the so-called Fail-Safe approach had not included a disciplined engineering evaluation of crack growth and residual strength characteristics of each principal structural element using fracture mechanics technology necessary to specify inspection methods, threshold and frequency which would detect damage prior to catastrophic failure. There had been a number of accidents in the mid seventies on aircraft designed to the Fail-Safe principle which may have been prevented had such inspections been imposed. Thus, in December, 1978 the FAA released amendment 45 to FAR 25.571 requiring that new structure be designed to "Damage Tolerant" principles unless it could be shown that this approach would be impractical whereupon a "Safe-Life" option could be used. In May, 1981 an advisory circular AC-91.56 was issued to provide guidance material for the issue of Supplemental Inspection Documents (SIDs) for existing Large Transport Category Airplanes. It was expected that advanced fracture mechanics principles would also be adopted to develop these SIDs. Thus, for both new designs and existing aircraft it is expected that engineering evaluation of the structure under typical load environmental spectra must show that catastrophic failure due to fatigue, accidental damage or corrosion will be avoided throughout the operational life of the aircraft. Over the last decade this process has been carried out. Inspection programs for both new designs and existing older aircraft have been based on a damage tolerance philosophy. However, up to the time of this writing, a system is not in place to require that all repairs or modifications to principal structural elements on these aircraft be evaluated to damage tolerance principles. Currently, the majority of these repairs are designed to an equal or better static strength requirement. Inspection procedures specified for the basic airplane are not being modified to reflect a change in design detail as a result of the repair or modification. Although the repairs or modifications may have equal or better static strength capability their effect on the fatigue quality and inspectability of the structure may be considerable. It is understood that a number of the major airframe manufacturers are currently working towards including damage tolerant evaluated standard repairs in their structural repair manuals. Others may follow this lead. This paper is intended to highlight this problem and perhaps outline some guidance to those occupied in aircraft modification and repair.

Degradation of Structure Due to Repair

In general, any repair to an airframe structure can substantially degrade fatigue life if extreme care in design detail is not taken. In the past, engineering evaluation of repairs has been based on equal or better static strength only without too much consideration for fatigue life. This philosophy can easily lead to static strength overdesign with consequent considerable loss in fatigue quality compared to the original structure. This phenomenon can easily be demonstrated analytically by considering a very simple example case. Figure

1a shows a typical fuselage skin element 0.04 inches thick riveted to a typical stringer. This element is subjected to cyclic hoop (circumferential) stress due to internal cabin pressure σ_h. Assume for our example this stress is 15 KSI with stress ratio R = 0. The fatigue life of this element will be based on the life at the row of rivet holes shown. These rivet holes are initially unloaded in the hoop direction. For our example case it will be assumed that the rivet holes have poor quality. This will be explained in detail later. The fatigue life of this row of rivet holes can be obtained from Figure 2 and as shown is about 160,000 cycles for 15 KSI with $\sigma_{br}/\sigma_{gr} = 0$. Suppose now we rivet a doubler to the skin as shown on Figure 1b. For our example we are not assuming any damage to the primary skin and we are not assuming the skin is cut. In other words we are not depending on all load being transferred out of the skin into the doubler. We are merely considering a doubler fastened to a piece of undamaged skin. Following the usual convention of increasing the doubler thickness one gauge, in the case of damaged skin, we will assume the doubler thickness is 0.05 inches. Whether we need it or not there will be load transfer out of the skin into the doubler due to strain compatibility between the two pieces. The two pieces are fastened together and will be attempting to strain together. The highest rivet loads, induced from the skin into the doubler, will be at the first row as shown in Figure 1b. Figure 1c illustrates the induced fastener load F in the skin reacted by the load F applied to the doubler. The gross stress σ_h, along line AB in Figure 1c, will be unchanged in the presence of the doubler but now we have induced a bearing stress in the hole σ_{br} which will degrade the fatigue life. This is illustrated by the various Sn curves of Figure 2. It can be seen that for constant amplitude stress the life is reduced with increasing σ_{br}/σ_{gr} ratio. The stress in the sheet will reduce to the bypass stress σ_{bp} and the stress in the doubler will increase to σ_d. In most cases the critical location for fatigue will be at row 1 in the sheet where the gross stress is still σ_h and the bearing stress in the sheet is highest due to the highest fastener load. In order to determine the fatigue life at this location it is necessary to determine the fastener loads in the first row. This is done through a displacement compatibility analysis of the joint.

A typical strip, as indicated in Figure 1b, is idealized as shown in Figure 3. Each rivet is simulated as an elastic spring under shear load and each portion of the skin and doubler strip is idealized as a bar. Bar displacements are obtained simply from equation 1:

$$\text{Bar displacement} \quad \delta_{bar} = PL/AE \qquad (1)$$

Where P = Bar load
L = Bar length
A = Bar area
E = Bar modulus

Rivet shear displacements are given by empirical equation 2 [1]:

$$\text{Rivet displacement} \quad \delta_{riv} = F[A+B(D/t_D + D/t_S)]/(ED) \qquad (2)$$

Where F = Rivet shear load
D = Rivet diameter
E = Sheet modulus
t_d = Doubler Thickness
t_s = Skin thickness
A = 5.0 for aluminum rivets and 1.666 for steel fasteners
B = 0.8 for aluminum rivets and 0.86 for steel fasteners

Displacements in the skin at each rivet are made compatible with those in the doubler after accounting for rivet displacement. Load compatibility is merely assumed, for example as:

$$P_{S1} - P_{S2} = F_1, \quad P_{S2} - P_{S3} = F_2 \quad \text{etc.}$$

and $$P_{D1} - P_{D2} = F_1, \quad P_{D2} - P_{D3} = F_2 \quad \text{etc.}$$

Where S and D denote skin and doubler.

The resulting load distribution in our example case is shown in Figure 4. It can be seen the highest loads are at the first row and are 187.2 lbs per rivet. The skin bearing stress is therefore 187.2/(0.04 x .19) = 24632 psi. Bearing stress to gross stress ratio σ_{br}/σ_{gr} = 24362/15000 = 1.642. The calculated life is therefore 53800 cycles as indicated by Figure 2. Thus, the addition of the 0.05 inch thick doubler, even though for our example case is not transferring load across a damage area, has caused a reduction in fatigue life from 160,000 cycles to 53,800 cycles because of load transfer from the skin into the doubler due to displacement compatibility. Figure 5 shows decreasing skin life with increasing doubler thickness obtained by similar analysis. Further reductions in skin life are shown when steel fasteners are used due to higher first fastener load due to increased stiffness.

It is shown in Figure 5 that the fatigue life of the skin is extremely sensitive to doubler thickness and that the life is controlled by the first fastener load. In order to provide some guidance to repairers and modifiers of airframe structure a number of typical configurations have been analyzed. Displacement compatibility analysis was performed to give critical fastener loads for a variety of skin doubler and lap splice combinations. Figure 6 shows the idealization used for the skin/doubler combinations. Sufficient rivets (5) were considered so that rivet load away from the doubler edge was insignificant. The rivet load distribution is shown in Figure 6 for a typical configuration assuming a unit 1 KSI applied gross stress. Strip and rivet displacements were based on equations 1 and 2 respectively. Figure 7 shows first and critical fastener load as a function of basic skin and doubler thickness for 1 KSI unit applied gross stress when 3/16 inch diameter aluminum rivets were assumed for the skin/doubler configuration. Figure 8 shows similar data when 3/16 inch diameter steel fasteners are assumed. Figures 9, 10 and 11 show critical fastener loads for 3, 4 and 5 rivet lap splices. Aluminum rivets, 3/16 inch diameter, were assumed for the lap

splice configurations.

In the case of the lap splice configurations represented by Figures 9, 10 and 11 the following rules will be helpful.

1) When t_2 is thinner than t_1 the first attachment load is the highest.

2) When t_2 is thicker than t_1 the last attachment load is the highest.

3) When t_1 and t_2 are equal the first and last attachment loads are equal.

Skin bearing stress σ_{br} can be calculated as a function of applied gross stress σ_{gr} from Figures 7 through 11. An estimate of conservative fatigue lives, not including local bending stresses due to eccentricity, can be made using this information along with open hole fatigue data shown in Figures 12, 13 and 14 for 2024-T3 material at stress ratios $R = \sigma_{min}/\sigma_{max}$ of -0.2, 0.0 and +0.2 respectively.

Figure 5 shows how overall fatigue life can be drastically reduced with increasing doubler thickness. Crack propagation life is also influenced by fastener load induced by transfer of load out of the skin into the doubler. However, the effect on crack growth life is not so great as on overall fatigue life. The effect of fastener load is a very localized effect taking place near the hole boundary. As the crack forms and starts to propagate the fastener bearing load becomes less significant in it's influence on the crack tip stress intensity factor. The major difference in overall fatigue life is created in the nucleation portion of the life when the crack is extremely small. The effect of doubler thickness on crack growth life is illustrated by Figure 15. This figure shows the number of constant amplitude cycles, at a gross stress of 15.0 KSI with stress ratio R = 0, to propagate a crack in a 0.04 inch thick by 1.0 inch wide strip of 2024-T3 material. The initial crack size is 0.02 inches on both sides of a 3/16 inch diameter hole and the final crack size is 0.35 inches on both sides of the hole. The table on Figure 15 shows some difference in crack growth life up to a doubler thickness of 0.05 inches but beyond this doubler thickness there is little difference. Induced fastener loads shown in Figure 15 assumed the configuration illustrated by Figure 7. It should be noted, however, that skin bending due to eccentricity of the load reaction due to doubler thickness is not accounted for. The curves on Figure 15 show the difference in life between a configuration with no doubler and one with a 0.05 inch thick doubler. This analysis was performed using the computer programs GEOFAC and LICAFF [2]. Forman's equation was used to represent the crack growth rate as follows:

$$da/dN = [4.372 \times 10^{-7} (\Delta K)^{2.7229}]/[(1-R)80 - \Delta K] \qquad (3)$$

Repaired Structure Life Improvement

It has been illustrated by previous examples that repairs can

drastically degrade fatigue life of basic structure. It was analytically demonstrated that this degradation is primarily due to first fastener induced load caused by displacement compatibility. This fastener load can be reduced and the fatigue life improved by tapering the doubler. The objective in tapering is to reduce the doubler thickness between the first and second fasteners. Merely tapering the doubler between the edge and the first fastener has no effect on reducing the first fastener load.
Figure 16 illustrates an example of how tapering can reduce the first fastener load. The fastener load distribution is compared to the original example case of 0.04 inch thick skin with a uniform 0.05 inch thick doubler. The reduced fastener load, resulting in a reduced bearing stress σ_{br} and therefore reduced σ_{br}/σ_{gr} ratio, results in a life of 59,000 cycles at a gross stress σ_{gr} of 15.0 KSI with R = 0. This is a life improvement of nearly 10% compared to the life of 53,800 cycles obtained for the uniform 0.05 inch thick doubler. It should be noted that these comparisons are being made with conservative open hole fatigue data. Greater improvements could be shown using fatigue Sn data representative of good quality riveting. However, this type of riveting is rare in field repaired structure usually due to space restrictions as will be discussed later.

Further reductions in first fastener load resulting in life improvement can be achieved if the typical 0.05 inch thick doubler is replaced by multiple doublers. This is usually easier to accomplish in field repairs anyway. As an example, a doubler system involving standard gauges of 0.025 inches and 0.032 inches were analyzed for comparison. The configuration is shown in Figure 17a. The 0.025 inch thick doubler is extended another fastener row. For this comparison strain compatibility analysis accounting for fastener flexibility results in first fastener load of 122.4 lbs resulting in skin bearing stress of 16.105 KSI and σ_{br}/σ_{gr} = 1.074. This results in a fatigue life of 70,500 cycles at a gross stress of 15.0 KSI. Thus, laminating the doubler increases the fatigue life by 31% over the life obtained for the example case using a single 0.05 inch thick doubler.

Improvements in Inspectability

Any repair doubler applied externally to the fuselage structure such as that shown in Figure 1(b) will degrade the external detectability of the skin at the critical fastener row. Skin cracking at the first fastener will be hidden externally by the repair doubler. Of course the skin will still be visually inspectable internally but then internal lining would have to be removed. Also external inspectability of this type of repair is still possible with more sophisticated low frequency eddy current NDI. The inspectability of the repair can be improved by placing the secondary doubler inside and the primary doubler outside as shown in Figure 17b.

Further improvements in external inspectability can be made by removing alternate fasteners at the first critical row to improve residual strength capability and increase multi-site-damage (MSD) critical crack sizes. For example, Figure 18 shows our laminated doubler case but with alternate fasteners in the

critical first row removed. This allows the net cross sectional area in the skin at the critical first fastener row to be increased. In the case of MSD in 2024-T3 material the residual strength is governed approximately by net section yield criteria between crack tips. Assuming net section yield governs the residual strength capability then the critical MSD crack size can be expressed as:

$$a_{cr} = [\sigma_y(P-D) - \sigma P]/[2(\sigma_y)] \quad (4)$$

Where σ_y = material yield strength
P = fastener spacing
D = fastener diameter
σ = applied gross stress

Assuming a B value of σ_y = 43.0 KSI for 2024-T3 unclad sheet material in the LT direction from MIL-HDBK-5 the residual strength diagram for the MSD case is shown on Figure 18 for P = 1.0 and 2.0 inches with rivet diameter 0.19 inches. It can be seen that the critical crack size is increased from 0.2306 with 1.0 inch fastener spacing to 0.5566 inches with 2.0 inch fastener spacing. This provides for increased detectability and longer crack growth life. However, the overall fatigue life will be decreased with this configuration. Displacement compatibility analysis indicates that when alternate fasteners are removed the remaining fasteners in the critical first row try to load up a wider strip of the secondary doubler thus increasing the first fastener load. Analysis for our typical example at an applied stress of 15 KSI indicates the first fastener load is increased from 122.4 lbs to 184.2 lbs. This increases the bearing stress to 24.237 KSI resulting in a bearing to gross stress ratio σ_{br}/σ_{gr} = 1.616. The resulting overall fatigue life becomes 54,500 cycles. Therefore removing alternate fasteners in the critical first row in the secondary doubler has degraded the overall fatigue life of the laminated configuration but considerably improved crack detectability.

The fatigue life can be improved by effectively tapering the inner doubler. This is done by fingering as illustrated by Figure 18. The fingers effectively reduce the inner doubler area between the first and second fastener rows thus relieving the first fastener load. This results in a lower skin bearing stress and improved crack initiation life. This configuration offers the highest fatigue life coupled with the best external detectability.
Remember, again the fatigue lives quoted are for open hole quality.

Riveting Quality

The fatigue initiation life of the basic skin in the presence of a repair doubler can be related to the quality of the riveting operation. If the rivets do not properly fill the hole after "bucking" then poor fatigue quality can be expected as reflected in the open hole fatigue data of Figures 12 through 14. Open hole fatigue data reflects a stress concentration factor, K_t, of approximately 3.0 for wide thin sheet when σ_{br}/σ_{gr} = 0. This concentration factor results when the boundary of the

rivet hole is allowed to deflect as illustrated in Figure 20(a). If the hole is filled with a pin capable of restraining the free boundary displacement of the hole then the stress concentration factor is reduced to approximately 2.0 as illustrated by Figure 20(b). This reduction in stress concentration factor at the hole boundary will result in improved fatigue life. Further reductions in effective stress concentration factor can be achieved if the rivet is bucked properly. Figure 20(d) illustrates that as the rivet is bucked it will swell in the hole and create the equivalent of an interference fit pin applying a radial pressure to the hole boundary which in turn creates local radial and tangential stresses in the sheet around the rivet. With little interference the material near the hole boundary becomes plastically deformed. It can easily be shown analytically how this effect can reduce the effective stress concentration factor at the hole boundary. Elastic-plastic stress analysis used in pressurized thick cylinders can be used to illustrate this effect. Using this theory it is possible to develop an equation relating the amount of interference to the radius of the plastic front as shown below:

$$2\mathrm{Ln}(\rho/r)+(1+\nu_s)/(1-\nu_r)(E_r/E_s)(\rho/r)^2 = I\sqrt{3}E_r/[2r\sigma_y(1-\nu_r)] \qquad (5)$$

This equation is solved by iteration for ρ/r. The value of ρ is then used to calculate the resulting stress distribution as follows:

Stresses in the elastic region

$$\sigma_{RP} = \sigma_y/\sqrt{3}[2\mathrm{Ln}(R/\rho) - 1] \qquad (6)$$

$$\sigma_{\phi P} = \sigma_y/\sqrt{3}[2\mathrm{Ln}(R/\rho) + 1] \qquad (7)$$

Stresses in the elastic region

$$\sigma_{RE} = \sigma_y/\sqrt{3}(\rho/R)^2 \qquad (8)$$

$$\sigma_{\phi E} = \sigma_y/\sqrt{3}(\rho/R)^2 \qquad (9)$$

Where σ_{RP} = radial stress in plastic region

$\sigma_{\phi P}$ = tangential stress in plastic region

σ_{RE} = radial stress in elastic region

$\sigma_{\phi E}$ = tangential stress in elastic region

I = diametral interference

r = hole radius

ρ = radius of plastic front

E_r = modulus of rivet material

E_s = modulus of sheet material

ν_r = Poisson's ratio for rivet material

ν_s = Poisson's ratio for sheet material

R = radius at which stresses are required

σ_y = material yield stress

Equation 5 was solved for diametral interference values, I, of 0.003 and 0.004 inches respectively to illustrate how proper rivet swelling can provide beneficial residual compressive stresses at the hole boundary. Rivet diameter was assumed to be 0.19 inches in 2024-T3 sheet material with yield strength equal to 43 KSI. Poisson's ratio in the plastic range was assumed to be 0.5. Figure 21 shows the resulting stress distribution in both plastic and elastic regions. The compressive residual stresses would be subtractive from the applied tension stresses effectively reducing the stress concentration at the hole boundary and subsequently improving the fatigue life. However, to obtain substantial interference the rivet must be bucked squarely. Very often, especially in field repairs where space may be restrictive, the rivets are not bucked squarely resulting in a "clinched" installation. This situation often occurs when the working space is restrictive not allowing the bucking bar to be held squarely. When clinching occurs the hole is not properly filled and rivet swelling does not occur. Thus the beneficial residual compressive stresses are not present. In fact, severe clinching can cause a situation where there may be a gap between the hole boundary and the rivet wall thus allowing some free boundary displacement as shown in Figure 20(a). When this occurs, reflective of poor quality riveting, the fatigue life will be more representative of open hole Sn data shown in Figures 12 to 14. Figure 22 shows an example of rivet clinching taken from an actual failed field repair. The sketch on Figure 22 illustrates the gap which can exist between the rivet and the hole boundary. This is graphically illustrated by Figure 23 which shows a cross sectioned purposely clinched rivet. The gap between the hole boundary and the rivet wall is clearly visible. Figure 24 illustrates the variation in fatigue life which can be expected with variations in riveting quality in 2024-T3 sheet at R = 0.

Figure 25 shows fatigue Sn data which may be reasonably expected with good quality 3/16 inch diameter rivets in 2024-T3 material where the riveting is square and hole filling but with no load transfer. This data is a little difficult to use in the presence of load transfer but this author has found the methods of Lars Jarfall [3,4] to be useful in obtaining an effective stress σ_{eff} which may be used with the Sn data of Figure 25 to approximate the fatigue failure life. By reviewing the work of Jarfall it is possible to determine an effective stress as follows:

$$\sigma_{eff} = [1.3K_{tbr}\ \sigma_{br} + K_{tbp}\ \sigma_{bp}]/K_{tbp} \qquad (10)$$

Where σ_{eff} = effective stress

σ_{br} = bearing stress

σ_{bp} = bypass stress

K_{tbr} = stress concentration factor relating peak stress at edge of hole to σ_{br}

K_{tbp} = stress concentration factor relating peak stress at edge of hole to σ_{bp}

Of course the study of Jarfall's results should be used to obtain the proper parameters but this author has found the following reduction of equation 10 to give reasonable results with Sn data of Figure 25 for good quality riveting. Again this data does not reflect possible bending in the joint due to eccentricities.

$$K_{tbp} = 3.2, \quad K_{tbr} = 1.4$$

$$\text{Therefore} \quad \sigma_{eff} = 0.569\sigma_{br} + \sigma_{bp} \tag{11}$$

Stresses in equations 10 and 11 are defined in Figures 12, 13 and 14.

It should again be pointed out that field repairs are very often not of the fatigue quality represented by Figure 25. If advise could be given it would be not to consider fatigue quality beyond that depicted by Figures 12, 13 and 14 for field repairs. Even then, a conservative scatter factor should be considered to establish threshold for future detailed inspection of the repair. The reason for including Figure 25 was mainly to illustrate the differences in fatigue life between good quality riveting and what may be expected in field repairs where access may not be as good as in the initial assembly of the airplane.

Degradation of Inspectability Due to Repairs

It has been shown how repairs can degrade the overall fatigue quality of the basic structure. It has also been shown that the most critical locations for future fatigue damage are in the basic skin at the first attachment row in the doubler. In addition to degradation in overall fatigue life the repair itself can degrade the inspectability of the basic structure considerably. In order to illustrate this assume that a crack growing in a basic fuselage skin becomes visually detectable with high reliability at say a half crack length of 0.5 inches. Assuming a constant amplitude cyclic stress of 15 KSI with stress ratio R = 0 with crack growth rate represented by Forman's equation 3, the crack growth life would be 29,600 cycles as illustrated by Figure 26. Now consider a repair doubler 9.0 inches long has been riveted to the basic skin. The most critical location for future fatigue damage is in the skin at the first row of fasteners. Still assuming the visual half crack length of 0.5 inches the skin crack would be able to propagate to a half crack length of 4.5 + 0.5 = 5.0 inches before it could be detected visually externally. Thus the safe inspectable crack growth life has been reduced from 29600 cycles to 1200 cycles. It can be seen that a doubler length slightly longer than 9.0 inches would leave no visually detectable life from an external inspection standpoint. Of course, a less desirable internal visual inspection could be adopted but this would require internal lining removal. Also a more sophisticated

low frequency eddy current inspection could be adopted. However, the more desirable external visual inspection capability could be completely degraded by this type of repair.

The external visual inspectability can be improved by including an internal doubler as indicated by Figure 27. This configuration was addressed in Figure 17 and shown to have improved fatigue life of 31% for our example case over the doubler type shown in Figure 26. The first fastener row in the internal doubler is critical for fatigue cracking in the skin. A crack propagating in the skin at this row will be externally detectable and so the crack growth life would be about 29600 cycles as shown by Figure 26 for our example case. The residual strength capability of this type of repair in the presence of multi-site damage can be improved by eliminating alternate fasteners in the critical row. This was indicated by Figure 18. Also the external visual detectability of this configuration would be improved like the straight edged internal doubler also shown on Figure 27. However there is a penalty on overall fatigue life by eliminating alternate fasteners. The purpose of the fingers, as previously explained, is to restore some of this fatigue life by reducing the first fastener loads through fingering or effectively tapering the internal doubler. The finger doubler repair is, in the opinion of the author, the best compromise for a permanent repair to basic fuselage structure.

Damage Tolerance Evaluation of Repairs

Current regulations mandate that repairs or modifications to commercial transport category airplanes which have been certified to the damage tolerance regulations FAR 25.571, or are operating under a Supplemental Inspection Document (SID), must be evaluated for damage tolerance. The reason for this is that the in-service structural safety of these aircraft is being managed through inspection programs based on a damage tolerance philosophy. Inspections for principal structural elements are developed through an engineering evaluation of crack growth and residual strength, both of which are extremely sensitive to geometry. Any change in the geometry of principal structural elements such as repairs or modifications can drastically change the threshold, frequency and method of inspection and can also effect the residual strength capability of the structure. Obviously the original manufacturers of the airplanes are in the best position to do this evaluation. They usually have the know-how and are in possession of all the structural loads and stress data necessary for such an evaluation. However, the current system is such that there are hundreds of repair stations, small modification companies, operators and private DERs who are involved in the repair and modification of airplane structures. In order to support the aging fleet over the next decade the number of these repair stations and small modification companies must increase. Information contained in a recent General Accounting Office (GAO) report on aging aircraft states that by the year 2000 there will be 4474 commercial transport airplanes, manufactured by Boeing, Douglas and Lockheed, world wide, which

will be operating beyond the initial 20 year life goal. The manufacturers of these airplanes will need considerable assistance to keep them operating safely and repaired. The small repairers and modifiers, currently performing repair analysis based on equal or better static strength only, will need to develop capability to perform damage tolerance evaluations. Conservative, simplified methods need to be developed to assist these small modifiers and repairers in performing crack growth and residual strength analysis in order to ease the burden on the major manufacturers. These manufacturers need to concentrate on producing new aircraft to replace the aging fleet. These statements are obviously over simplified. Exact damage tolerance evaluation is an extremely sophisticated process requiring experts in fracture mechanics who must also be experts in basic airframe stress analysis. The number of these experts in the industry is small and the job over the next decade will be overwhelming unless we do something about it now. As a first step, then, simplified methods need to be developed that will enable hundreds of modifiers and repairers to perform conservative analysis to support inspection programs for repairs and modifications. It is the opinion of the author that all repairs receive 100% continual inspection beyond a conservative threshold. Because of operational schedules and the economic need to keep airplanes flying the repair system may have to be in two stages. Immediate temporary repairs good for a limited time followed by permanent repairs supported by a damage tolerance evaluation. The greatest problem to the small modifier in performing damage tolerance evaluations is crack growth analysis. This generally needs original manufacturers load and stress data. Residual strength evaluation is not necessarily a considerable problem to a good fracture mechanics analyst since this falls into the same category as equal or better static strength analysis. ie the residual strength can usually be assessed from a knowledge of the airframe geometry. The first step then is to develop simplified, conservative, crack growth analysis methods. This of course has been done to some extent by a number of researchers. The most appealing method, at least to this author, is the method developed by Boeing's Damage Tolerance Technology group. Sufficient information exists in the literature [5, 6, 7, 8, 9] to provide an outline of the method. Some of the necessary data needed to complete this method does not exist in the open literature but this data can be readily developed with some effort.

Development of a simplified crack growth method

In general a crack growth analysis requires the solution of the following equation:

$$N = \int_{a_i}^{a_f} da/[F(\sigma_{max},R,a,M,G,\sigma_y)]$$

Where σ_{max} = maximum applied stress
R = stress ratio $\sigma_{min}/\sigma_{max}$
a_i = initial crack length
a_f = final crack length
M = material influence

G = geometric influence
σ_y = material yield strength

The majority of large airplane manufacturers have developed sophisticated numerical integration crack growth computer programs to solve this equation for a variety of materials and geometries and load spectra variations. These programs are being used to design new aircraft to meet the damage tolerance regulations and in some cases to develop SIDs for aging aircraft. Some manufacturers are using these methods to assess standard repairs with a view to updating their structural repair manuals. The crack growth method developed by Boeing allows rapid development of crack growth curves. Boeing has added sophistication to this method by considering load sequence effects under spectrum loading. It is the opinion of this author that for a conservative analysis of repairs additional sophistication needs to be left to the large manufacturers at this stage. The following is an outline of the development of the Boeing method but with parameters altered to fit in with familiar fracture mechanics methodology. The development here neglects the sophistication of load sequence effects included in the Boeing approach and which generally produce more accurate and less conservative results. In other words crack growth retardation is not included in the following approach. The approach is made possible through the following basic assumptions:

- Walker type simulation of crack growth rate data
- Separation of geometrical effects from stress and material so that integration of geometrical effects can be performed separately
- Standardization of complex randomized load spectra into a single repeatable flight
- Simulation of this single flight by a single constant amplitude cycle with zero stress ratio
- Subsequent constant amplitude crack growth analysis to produce a crack growth versus flights curve.

The Walker crack growth equation is expressed as:

$$da/dN = C((1-R)^q K_{max})^P \qquad (12)$$

The parameters for this equation are defined on Figure 28. The equation is basically a straight line equation when plotted on Log-Log paper. When da/dN is plotted against the effective stress intensity factor range, $K_{eff} = (1-R)^q K_{max}$, a single line is produced as shown to the left of Figure 28. Plotting da/dN as a function of the true stress intensity factor range, ΔK, allows several lines at different stress ratio, R, to be drawn as shown to the right of Figure 28. The width of the band of lines is controlled by the exponent q on the (1-R) term. This enables a better fit to be made of the test data points. The value of P is the slope of the lines as indicated.

Inverting equation 12 gives:

$$dN/da = 1/C\{(1-R)^q K_{max}\}^{-P}$$

$$N = \int_{a_i}^{a_f} 1/C\{(1-R)^q K_{max}\}^{-P}\, da$$

$$N = 1/C\{(1-R)^q\}^{-P} \int_{a_i}^{a_f} (K_{max})^{-P}\, da$$

Substituting for K_{max}:

$$N = \underbrace{1/C\{1/[\sigma_{max}(1-R)^q]\}^P}_{\text{load and material terms}} \underbrace{\int_{a_i}^{a_f} da/(\sqrt{\pi a}\,\beta)^P}_{\text{geometry terms}}$$

$$\text{let} \quad G^{-P} = \int_{a_i}^{a_f} da/[(\sqrt{\pi a}\,\beta)^P]$$

$$\text{Then } N = 1/C\{\sigma_{max}(1-R)^q\}^{-P} G^{-P}$$

$$\text{Or } N = 1/C\{1/[G\sigma_{max}(1-R)^q]\}^P \tag{13}$$

$$\text{Where} \quad G = \{ \int_{a_i}^{a_f} da/[(\sqrt{\pi a}\,\beta)^P]\}^{-1/P} \tag{14}$$

Equation 13 gives the number of cycles N to propagate a crack from an initial size a_i to a final size a_f with the effects of geometry defined by equation 14.

The term G will depend on the geometrical configuration. The results of equation 14 for all possible geometries is not included in the literature given by references [5, 6, 7, 8, 9,]. However, this term can easily be obtained by numerical integration for each specific geometry. There are many references in the literature providing the term β or the effect of geometry on the stress intensity factor K. For example, one of the most comprehensive of these is reference [10]. All other terms in equation 14 are defined.

Only in the simplest of cases can equation 14 be analytically integrated, for example, in the case of an infinitely wide unstiffened panel, where = 1.0.

$$G^{-P} = \int_{a_i}^{a_f} (\sqrt{\pi a})^{-P}\, da \qquad = \pi^{-P/2} \int_{a_i}^{a_f} (a)^{-P/2}\, da$$

$$\text{Therefore} \quad G^{-P} = (\pi)^{-P/2} \left[\frac{a^{1-P/2}}{1-P/2}\right]_{a_i}^{a_f}$$

$$G = \left\{(\pi)^{-P/2} \left[\frac{(a_f)^{1-P/2} - (a_i)^{1-P/2}}{1-P/2}\right]\right\}^{-1/P}$$

Figure 29 shows a plot of this equation for two values of a_f. There is a need to develop figures such as Figure 29, based on equation 14, for a variety of typical geometries by numerical integration.

For the benefit of those not familiar with this approach consider the case of a through crack in a panel of finite width 20.0 inches. The value of β for this case is generally accepted to be $[\text{Sec}(\pi a/W)]^{1/2}$ reference [11]. From equation 14

$$G^{-P} = \int_{a_i}^{a_f} (\sqrt{\pi a}\,\beta)^{-P}\, da$$

Therefore for our example case

$$G^{-P} = \int_{a_i}^{a_f} \{\sqrt{\pi a}[\text{Sec}(\pi a/W)]^{1/2}\}^{-P}\, da \qquad (15)$$

Now we need to plot the term $\{\sqrt{\pi a}[\text{Sec}(\pi a/W)]^{1/2}\}^{-P}$ as a function of a. Figure 30 shows this plot for $a_i = 1.0$ to $a_f = 4.0$ for our 20 inch wide panel example. In this case the slope of the da/dN curve, P, for aluminum alloy has been assumed 3.7. This value will vary from alloy to alloy but a value of 3.7 is a reasonable average value to use for aluminum. We now need a plot of G versus initial crack size a_i. Assume for a start $a_i = 1.0$. The value of G^{-P} will be the area under the curve ABCDEFGH shown in Figure 30. This can be obtained either by the mid-ordinate or Simpson's rule. For our case this value is approximately 0.09345. Therefore $G = [0.09345]^{-1/3.7} = 1.89767$. Similarly for $a_i = 2.0$ the value of G^{-P} will be the area under the curve BCDEFG. For our case this is approximately 0.02948. Therefore $G = [0.02948]^{-1/3.7} = 2.59204$. Using this simple approach a curve of G versus a_i can be plotted. The result for our case of a 20 inch wide panel is shown on Figure 31. This procedure to obtain a plot of G can be used for any complex geometry provided the term β, as a function of crack size a, is known. As mentioned previously β can be found for many geometries in the literature.

A useful tip to consider is that the term $(\sqrt{\pi a}\,\beta)^{-P}$ can be integrated in pieces. Therefore, for example:

$$G^{-P} = \int_{a_i}^{a_f} (\sqrt{\pi a}\,\beta)^{-P}\, da = \int_{a_i}^{a_1} (\sqrt{\pi a}\,\beta)^{-P}\, da + \int_{a_1}^{a_2} (\sqrt{\pi a}\,\beta)^{-P}\, da +$$

$$\int_{a_i}^{a_f} (\sqrt{\pi a}\,\beta)^{-P}\, da \quad \text{etc}$$

This is illustrated by Figure 32.

Therefore $G^{-P} = [G_1^{-P} + G_2^{-P} + G_3^{-P}]$ or $G = [G_1^{-P} + G_2^{-P} + G_3^{-P}]^{-1/P}$

In this case G_1^{-P} is the area under the curve ABGH, G_2^{-P} is the area under curve BCFG and G_3^{-P} is the area under curve CDEF. The usefulness of being able to integrate the geometrical term G^{-P} in pieces is best illustrated if one considers that the objective of a crack growth analysis is to produce a crack growth versus cycles curve. In this case it is an advantage to plot a G curve for the maximum value of a_f expected. This single curve can then be used to obtain G for lower values of a_f. This concept is illustrated by Figure 33. For example if we have a curve of G having been developed for a_f = 8.0 as shown to the left of Figure 33 but we want to consider crack growth from a_i = 1.0 to a_f = 6.0 we can say:

$$G[6.0 - 1.0] = \{(G[8.0 - 1.0])^{-P} - (G[8.0 - 6.0])^{-P}\}^{-1/P} \qquad (16)$$

Terms similar to G[6.0 - 1.0] mean G obtained between the limits 1.0 to 6.0. We can obtain the respective values of G[8.0 - 1.0] and G[8.0 - 6.0] from the curve to the left of Figure 33 and use these values in equation 16 to obtain G[6.0 - 1.0]. This is possible since $\{G[8.0 - 1.0]\}^{-P}$ is the integral of $(\sqrt{\pi a}\,\beta)^{-P}$ between the limits 1.0 and 8.0 which is the area of the curve shown to the right of Figure 33 represented as ABCDEF. Similarly $\{G[6.0 - 1.0]\}^{-P}$ is the integral of $(\sqrt{\pi a}\,\beta)^{-P}$ between the limits 1.0 to 6.0. Since the curve to the left of Figure 33 is based on the upper limit of 8.0 only then we use this to obtain G[6.0 - 1.0] by subtracting area BCDE from area ABCDEF and this is equivalent to area ABEF representing $\{G[6.0 - 1.0]\}^{-P}$. We then raise this area to the power -1/P and this represents G[6.0 - 1.0].

Expanding the concept illustrated by Figure 33 we can calculate more points on the crack growth curve if we only have one curve of G versus a_f by the same procedure. Figure 34 illustrates the procedure for 4 points on a typical crack growth curve. The term $\{G[8.0 - 1.0]\}^{-P}$ represents the entire area under the curve of $(\sqrt{\pi a}\,\beta)^{-P}$ from 1.0 to 8.0 shown to the right of Figure 33. The number of cycles to propagate the crack from 1.0 to other crack lengths are obtained by subtracting the remaining area of the curve of $(\sqrt{\pi a}\,\beta)^{-P}$ beyond the crack length required as illustrated in Figure 34. The values of G again are obtained from the G versus a_i curve as illustrated by the curve to the left of Figure 33.

To simplify the crack growth analysis under spectrum loading the first assumption is to assume all flights are similar. That is the crack is propagating under a single repeatable flight. This assumption is more reasonable for commercial transport aircraft than it would be for say a military fighter. This single repeatable flight is then simulated to a single cycle having the same crack growth as the repeatable flight.

From equation 13 $N = 1/C\{1/[G\sigma_{max}(1-R)^q]\}^p$

Or $N = 1/(CG^p)\{1/[\sigma_{max}(1-R)^q]\}^p$

Crack growth per cycle

$$1/N = CG^p\{\sigma_{max}(1-R)^q\}^p \quad (17)$$

Consider a single repeatable flight as shown in Figure 35. The total crack growth for this flight can be calculated using equation 17 by summing the growth for each cycle. It is usual practice to truncate the negative stresses so the cycles considered are those represented by the heavy lines between dots on Figure 35. However, some prefer to leave in the negative stresses, take the full range of stress from negative to positive, and then use the appropriate crack growth rate corresponding to the negative R ratio. There is usually very little difference between the two results. The total crack growth for the single flight is therefore:

$$T = CG^p \sum_{i=1}^{i=n} \{\sigma i_{max}(1-R_i)^q\}^p \quad (18)$$

The stress level S is then obtained, at a stress ratio R = 0, which will give the same crack growth as the single flight. This can be obtained by substituting R = 0 and $\sigma_{max} \approx S$ into equation 17. Therefore the growth for the single cycle is:

$$C(GS)^p \quad (19)$$

We can equate equations 18 and 19 to obtain the value of S:

$$CG^p \sum_{i=1}^{i=n} \{\sigma i_{max}(1-R_i)^q\}^p = CG^p(S)^p$$

Therefore $S = [\sum_{i=1}^{i=n} \{\sigma i_{max}(1-R_i)^q\}^p]^{1/p}$

$$S = [\{\sigma 1_{max}(1-R_1)^q\}^p + \{\sigma 2_{max}(1-R_2)^q\}^p + \text{etc.}]^{1/p} \quad (20)$$

This value of S, at a stress ratio R = 0, is substituted into equation 13 to obtain the number of cycles to propagate the crack from a_i to a_f with G determined for a_i to a_f.

Therefore $N = 1/C\{1/[GS]\}^p$

Or $N = 1/C(GS)^{-p}$ (21)

Crack Growth Evaluation of Specific Repair

Simplified methods to allow small repairers and modifiers to develop crack growth curves have been discussed. However, even to perform this simplified analysis it is necessary to have a

knowledge of stress levels in the basic structure. Without this knowledge it is impossible to perform even a simple damage tolerance evaluation. If, however, a crack growth curve for a particular element, prior to repair, were available then it may be possible to use this information to obtain a crack growth curve for the modified structure. Consider the very simple example of an original structural element as shown in Figure 36a which may be the vertical web of a wing spar cap. This element may have been repaired by adding a reinforcement strap as shown by Figure 36b perhaps to replace corroded material. If the original element had been classified as a principal structural element in the initial damage tolerance evaluation, performed to either certify the airplane or to develop the SID, then a crack growth curve must have been developed by the manufacturer. This curve may have been generated using a more sophisticated cycle-by-cycle crack growth analysis method including the effects of retardation and using a particular equation to simulate da/dN. What is needed is to determine the constant amplitude stress level S at a R ratio of zero which will match the crack growth curve for the original element. This would be done by calculating G for the original configuration using equation 14 and then varying S in equation 21 to match the overall crack growth life covered by the original crack growth curve. There are some minor problems associated with this approach. A very simple example will help illustrate these problems. Suppose the original stress spectrum for the element shown in Figure 36a was as illustrated in Figure 37. This has been simplified to illustrate a point. Suppose the existing crack growth curve were based on an initial 0.05 inch crack at one side of a hole as shown on Figure 36a. Suppose the original crack growth curve was based on Forman's equation given by equation 3. Crack growth retardation may have been accounted for using the Willenborg model [12]. The resulting crack growth curve, produced by RECYCL [2], would be as shown on Figure 38 curve A. Now if equation 21 were used to match the overall life for this curve, using equation 14 for G, and varying the stress level S in equation 21, then a life match would be established at a stress S of 19.45 KSI using a Walker equation with C = 3.88×10^{-10}. The value of C is not important since the same value would be used to generate a crack growth curve for the modified structure. The resulting curve is illustrated by curve B on Figure 38. Even though the overall life has been exactly matched the shape of this curve is not the same. The primary reason for this is that retardation was considered to develop curve A and the peak stress of 17 KSI in the spectrum created a plastic zone at the crack tip which effected the growth of subsequent cycles and reduced the slope of the crack growth curve when the crack was small. Since retardation was not considered for curve B the slope at the start of the curve was greater. If the original curve had been generated neglecting retardation effects but using the same Forman's equation 3 then the result would be as shown by curve C, developed by LICAFF [2], on Figure 38. Again using the value of G developed from equation 14 and varying the stress level S in equation 21, the overall crack growth life would be matched at a stress of 22.43 KSI using the Walker constant C = 3.88×10^{-10}. The resulting curve is shown as curve D on Figure 38. Now it can be seen that the shape of this curve is a closer fit to the curve developed under spectrum loading

without the effects of retardation. The slight difference in shape is due to the differences in the crack growth equation used. The Forman equation, used to generate curve C, is not a straight line equation as is the Walker equation. The spectrum analysis without retardation was repeated using the Walker equation with $C = 3.88 \times 10^{-10}$, $q = 0.6$ and $P = 3.7$. The results are shown on Figure 39. Equation 21 was then used to match this curve and a perfect match was achieved at a constant amplitude stress of 19.95 KSI. This match is illustrated by the points on the curve. The purpose of determining the constant amplitude stress level S which matches the original curve is to use this stress in equation 21 to develop a crack growth curve for the modified element. This would be done by calculating G for the modified element accounting for load transfer at the first rivet and the loss in visual detectability when the crack is under the doubler. Equation 14 would be used to develop the new G value based on standard stress intensity expressions found in the literature. This procedure would allow a crack growth curve for the modified structure to be developed without a knowledge of the original stresses but with a knowledge of the original crack growth curve. The purpose of Figure 38 was to illustrate that some caution must be exercised when using this procedure because of the possible mismatched shape illustrated by Figure 38 curves A and D. For example the matching curve B reflects a longer crack growth life from a detectable crack to critical if the detectable size is larger than the initial crack size used to produce the curve. For example, if the detectable size was considered to be 0.15 inches (say) the safe crack growth life from the original curve is 19000 flights but is 35000 flights using the matched curve. Because of this it is better to determine S in equation 21 to fit the curve from the detectable size to the critical size.

Future Possibilities

A method to generate crack growth curves for the modified or repaired structure was discussed using a very simple example case. The approach required a knowledge of the original crack growth curve. Without this curve or a knowledge of the original stress spectrum it is impossible to obtain the required information. One possibility requiring some limited research may be to divide the airplane structure into a number of zones, perhaps six or eight zones for the fuselage, the lower wing surface and the horizontal stabilizer tension surface. Standard conservative stress spectra could be developed, perhaps using the standard TWIST spectrum, for the most critical points in each zone. This could be done using the most conservative 1g and 1P stresses to be found anywhere in the industry. These standard spectra would then be used along with the simplified methods discussed to produce conservative crack growth curves and inspection intervals. The only alternative to this is to persuade the original manufacturer, with all his knowledge of the original stress spectra and loads, to perform the analysis.

Conclusions

- Any repair to an airframe structure has the potential to drastically degrade fatigue life and damage tolerance

capability.

- In most cases the critical location for future fatigue initiation is in the basic skin at the first fastener row in the repair doubler.

- Curves are presented illustrating degradation in fatigue life of the basic structure as a function of repair doubler thickness.

- Fatigue life of the basic structure can be calculated as a function of applied gross stress and bearing stress in the skin at the first fastener row.

- Curves are presented, based on displacement compatibility analysis accounting for fastener flexibility, which will enable the critical fastener loads to be determined as a function of skin and doubler thickness for five common repair configurations.

- Data from these curves, together with conservative Sn curves provided, will allow a repairer or modifier to assess the fatigue quality of the repair.

- Some ideas are provided which will enable improved fatigue life and inspectability by laminating the repair doubler.

- Simplified methods which may enable a small modifier or repairer to develop crack growth curves for the basic structure after repair are discussed.

Bottom Line

- All repairs to principal structural elements on aircraft certified to FAR 25.571 amendment 45 or on aircraft assessed to AC 91-56, where a SID document exists for the airplane, must be evaluated for damage tolerance.

- New inspection methods/thresholds/frequencies must be established for the repaired structure.

- The repaired airplane should be inspected at the determined frequencies after the established threshold.

Note

The opinions expressed in this paper are those of the author and not necessarily those of the FAA. The author is an advisor to The Aircraft Certification Service who have final authority.

References

[1]. Swift, T., "Damage Tolerance Analysis of Redundant Structures," Fracture Mechanics Design Methodology, AGARD-LS-97, North Atlantic Treaty Organization, London, England, Jan. 1979, pp. 5-1.

[2] Computer programs LICAFF, GEOFAC and RECYCL, FractuREsearch Inc. 9049 Cupstone Drive, Galena, Ohio 43021, USA.

[3] Jarfall, Lars., "Optimum Design of Joints: The Stress Severity Factor Concept," Aircraft Fatigue Proceedings of the 5th ICAF Symposium, Melbourne, Australia, 22-24 May, 1979.

[4] Jarfall, Lars., "Fatigue Cycling of Riveted or Bolted Joints," FFA report HF-1239. The Aeronautical Research Institute of Sweden, June 1969.

[5] Craig, L., and Goranson, U.G., "Airworthiness Assessment of Boeing Jet Transport Structures." Presented at the 10th ICAF Symposium, Brussels, Belgium, May 16-18, 1979.

[6] Goranson, U.G., and Hall, J., "Airworthiness of Long-Life Jet Transport Structures." Presented to the Royal Aeronautical Society Spring Convention on Long-Life Aircraft Structures, London, England, May 14-15, 1980.

[7] Craig,L., et al "Airworthiness of Long-Life Jet Transport Structures." Presented at the Air Transport Association of America Forum, Miami, Florida, October 1-3, 1980.

[8] Goranson,U.G., et al "Long-Life Damage Tolerant Jet Transport Structures." Presented at ASTM Symposium "Design of Fatigue and Fracture Resistant Structures," Bal Harbor, Florida, Nov. 10-11, 1980.

[9] Gunther, C.K., and Goranson, U.G., "Spectrum Loading Effects on Crack Growth in Major Components of Commercial Transport Aircraft." Presented to the International Conference on Application of Fracture Mechanics to Materials and Structures, Freiburg, Germany, June, 1983.

[10] Rooke, D., and Cartwright, D., "Compendium of Stress Intensity Factors." Printed in England for Her Majesty's Stationary Office by The Hillingdon Press, Uxbridge, Middx. England, Sept 1974.

[11] Feddersen, C.E., "Evaluation and Prediction of the Residual Strength of Center Cracked Tension Panels." Published in "Damage Tolerance in Aircraft Structures," ASTM STP 486, May 1971.

[12] Willenborg, J., Engle, R.M. and Wood, H.A., "A Crack Growth Retardation Model Using An Effective Stress Concept." US Air Force Tech. Memo. 71-1-FBR. Jan. 1971.

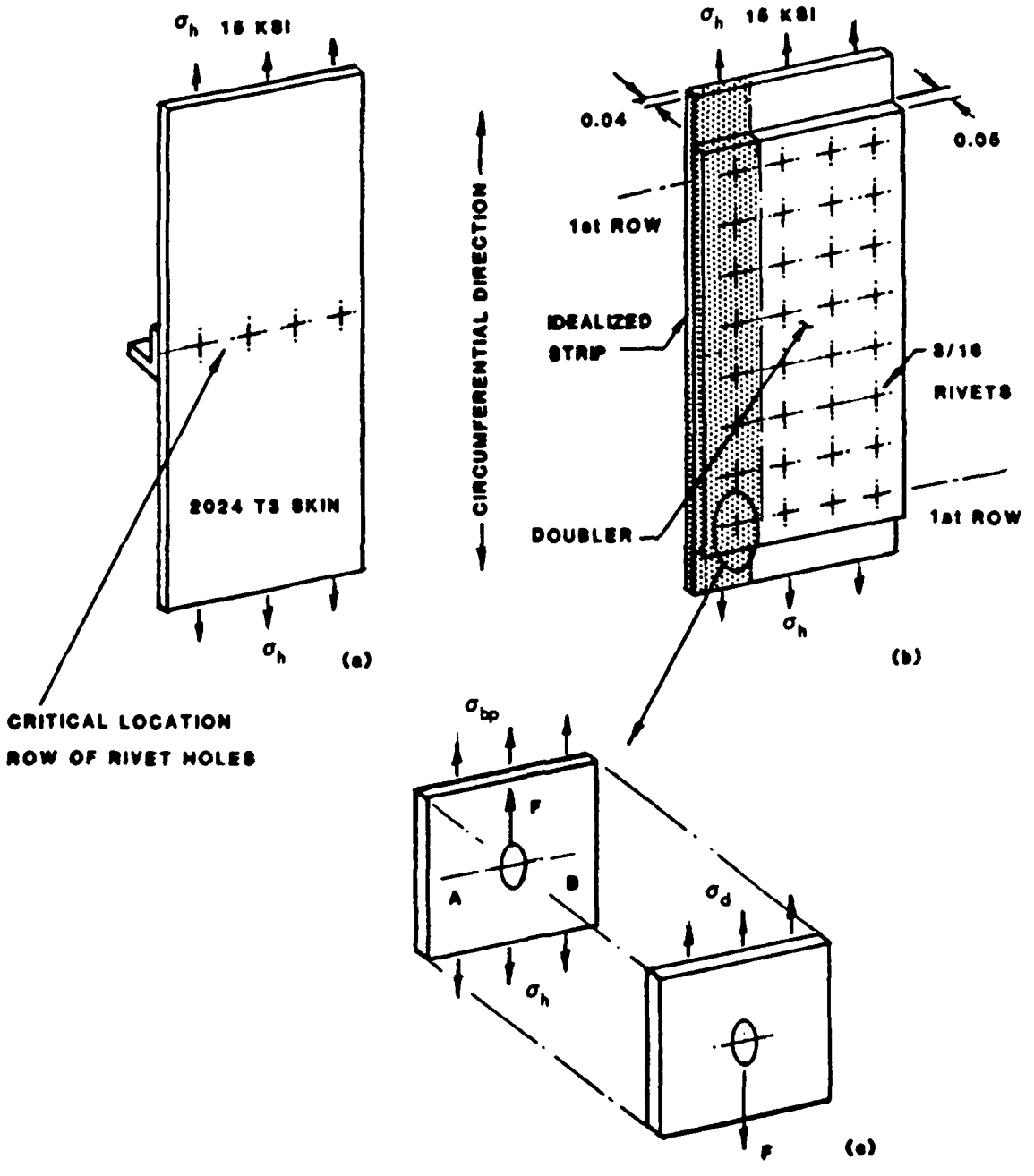

Fig. 1. Example of Doubled Element

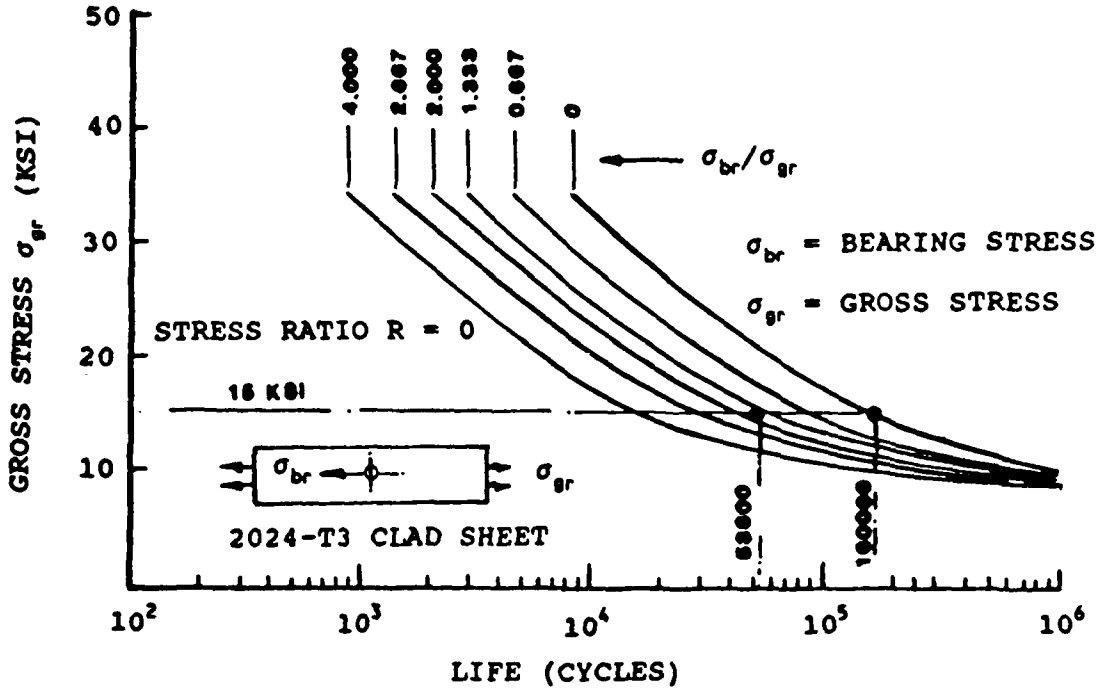

Fig. 2. Open Hole Sn Data 2024-T3

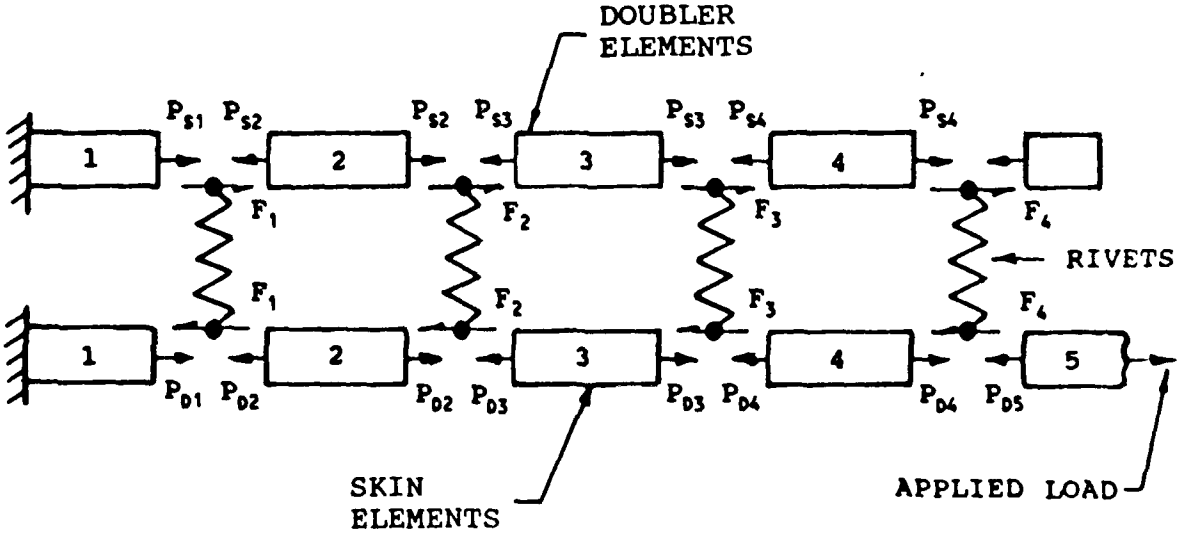

Fig. 3. Idealization of Strip

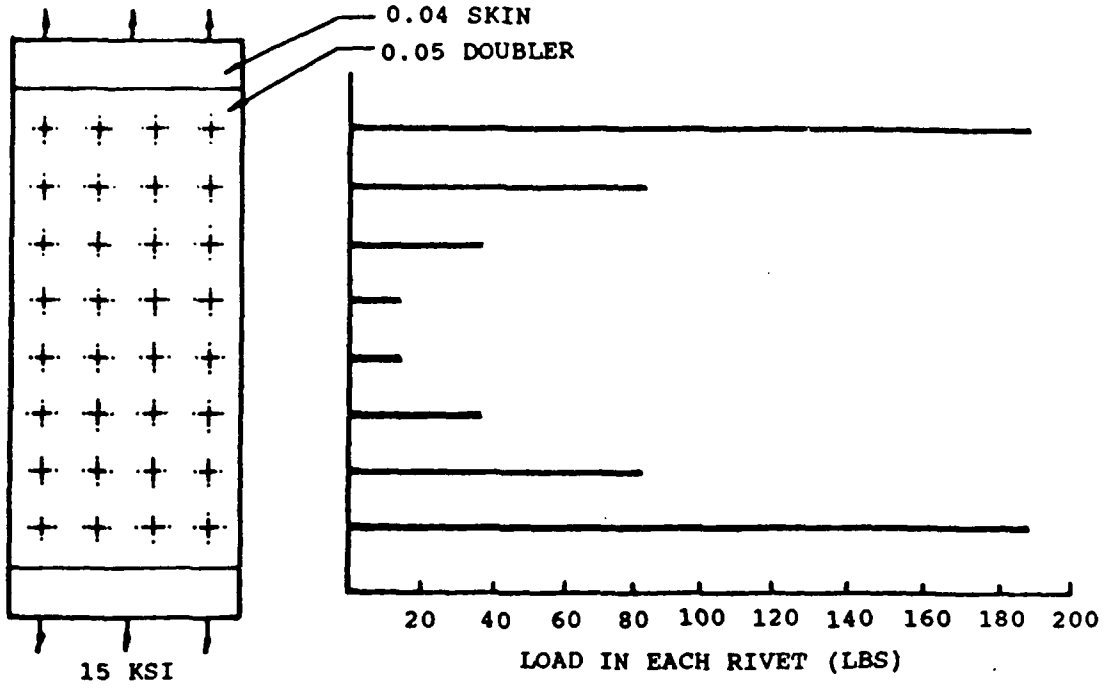

Fig. 4. Rivet Load Distribution For Example Case

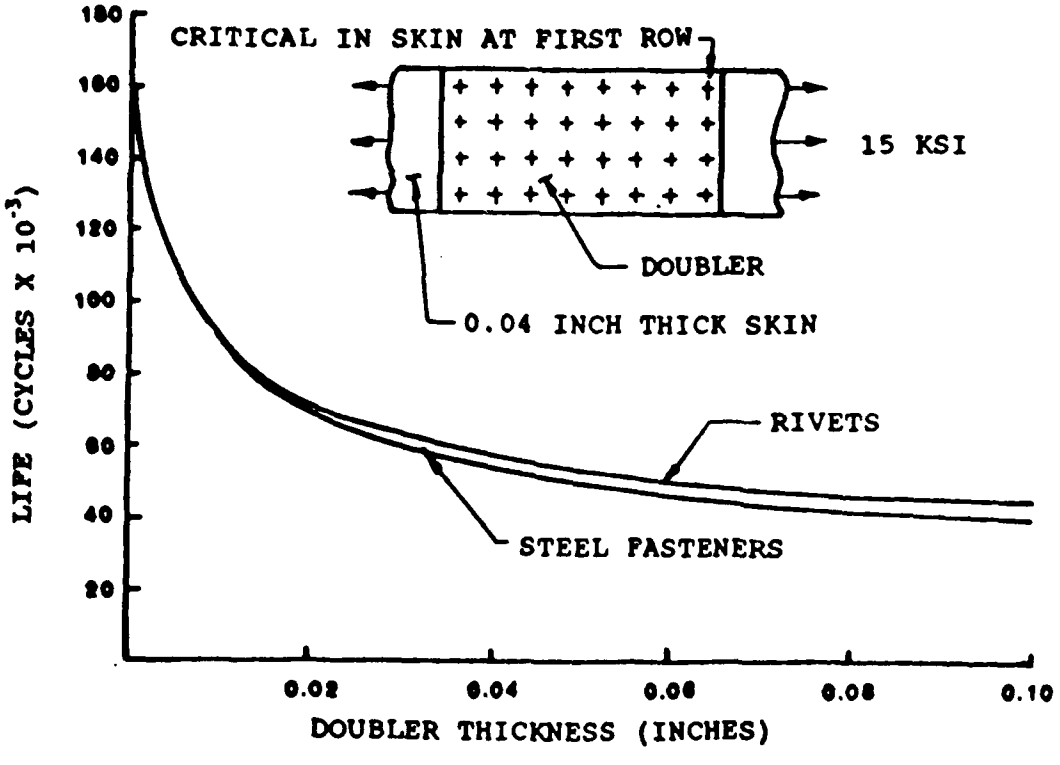

Fig. 5. Skin Fatigue Life At First Fastener

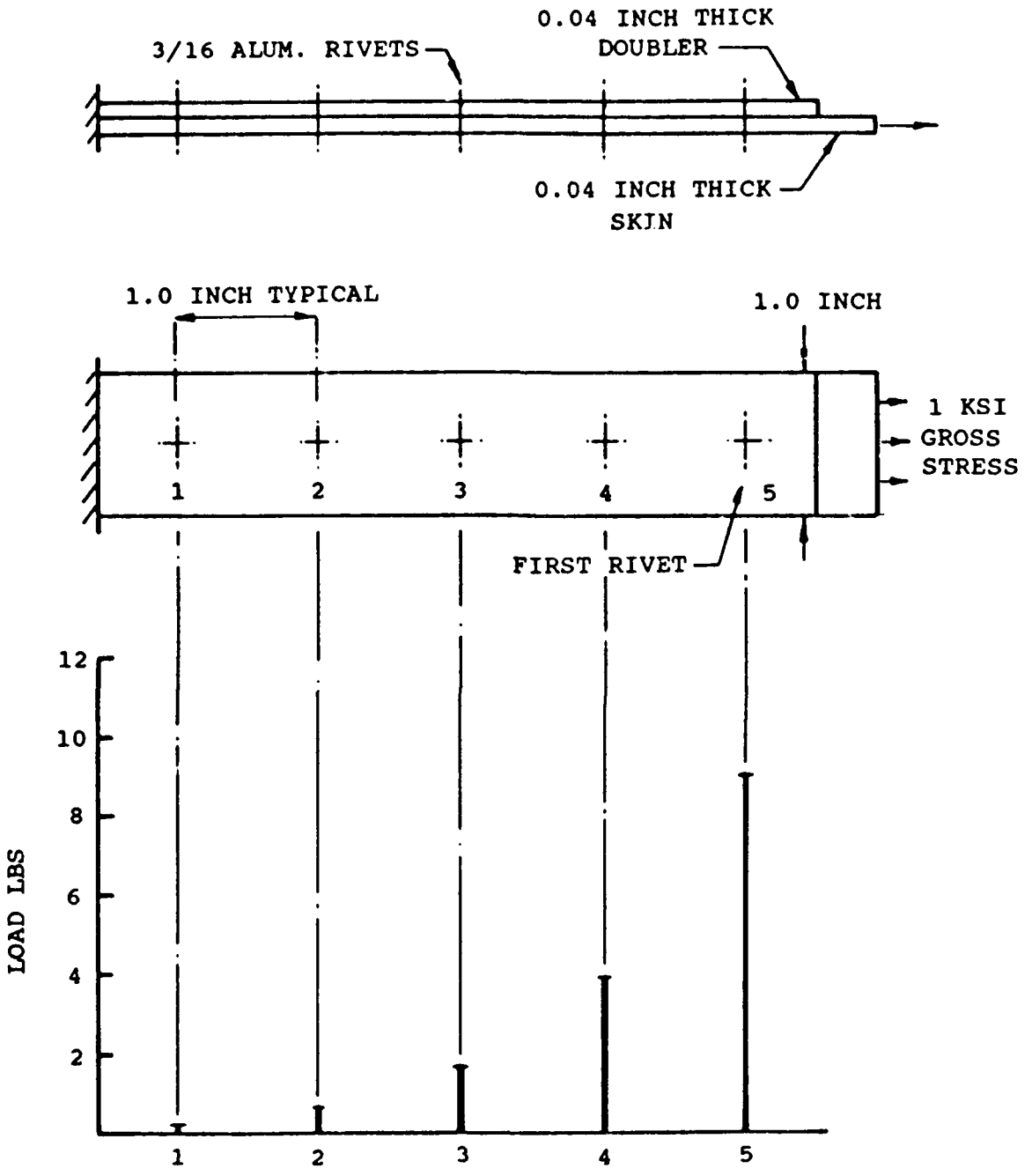

Fig. 6. Rivet Load Distribution in a Example Idealized Strip

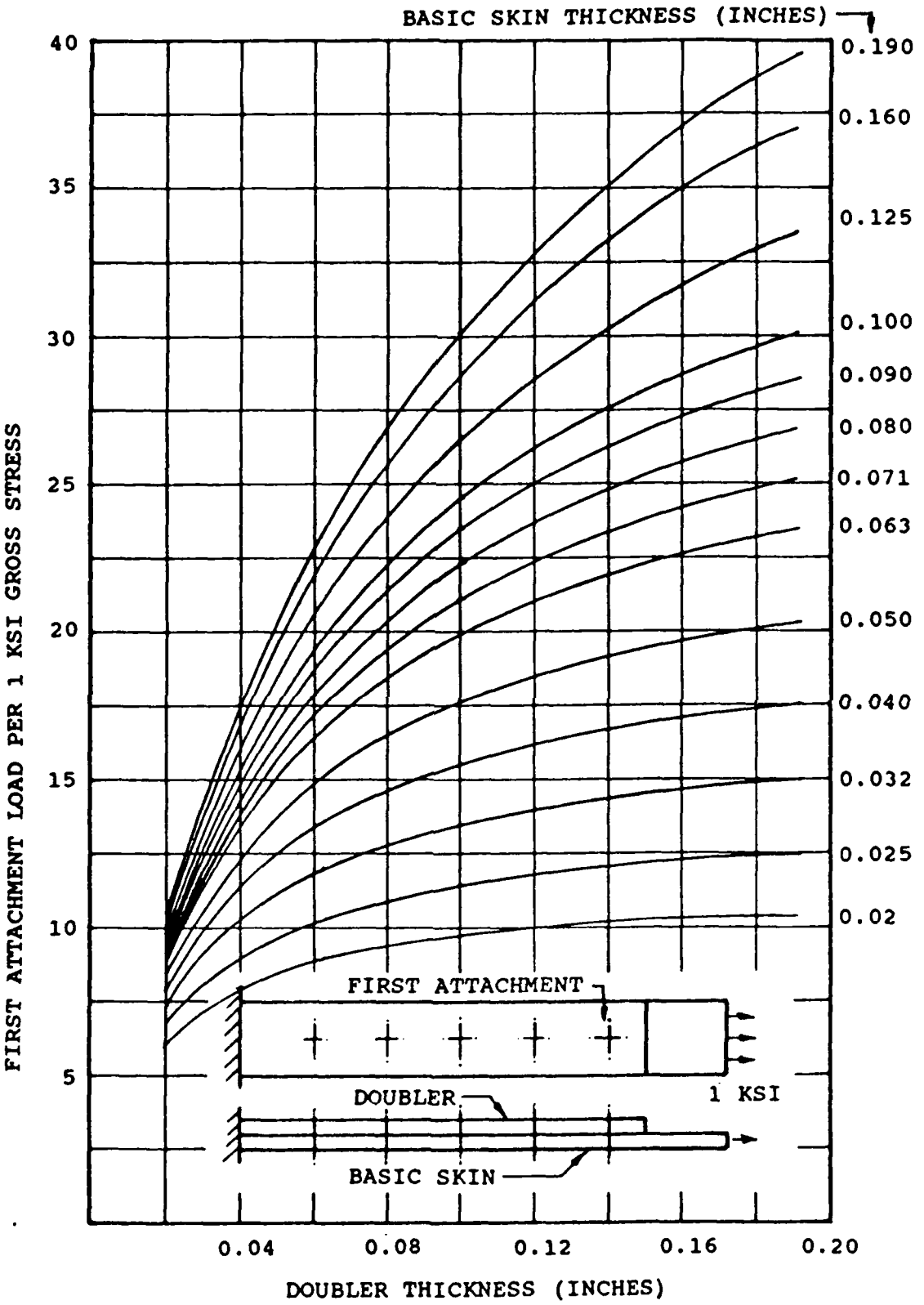

Fig. 7. First Fastener Load Per 1 KSI Gross Stress - 3/16 Inch Diameter Aluminum Rivets

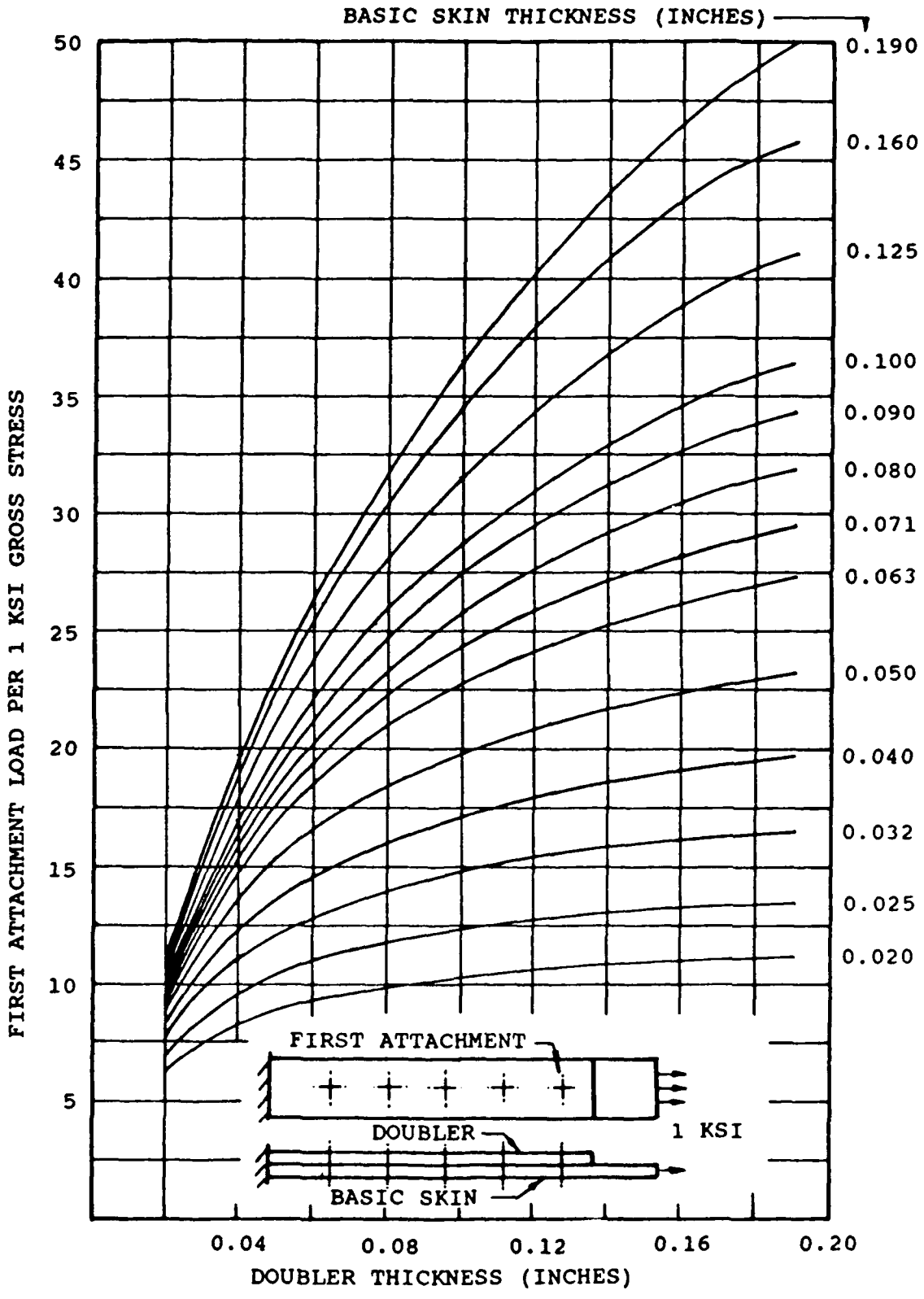

Fig. 8. First Fastener Load Per i KSI Gross Stress - 3/16 Inch Diameter Steel Fasteners

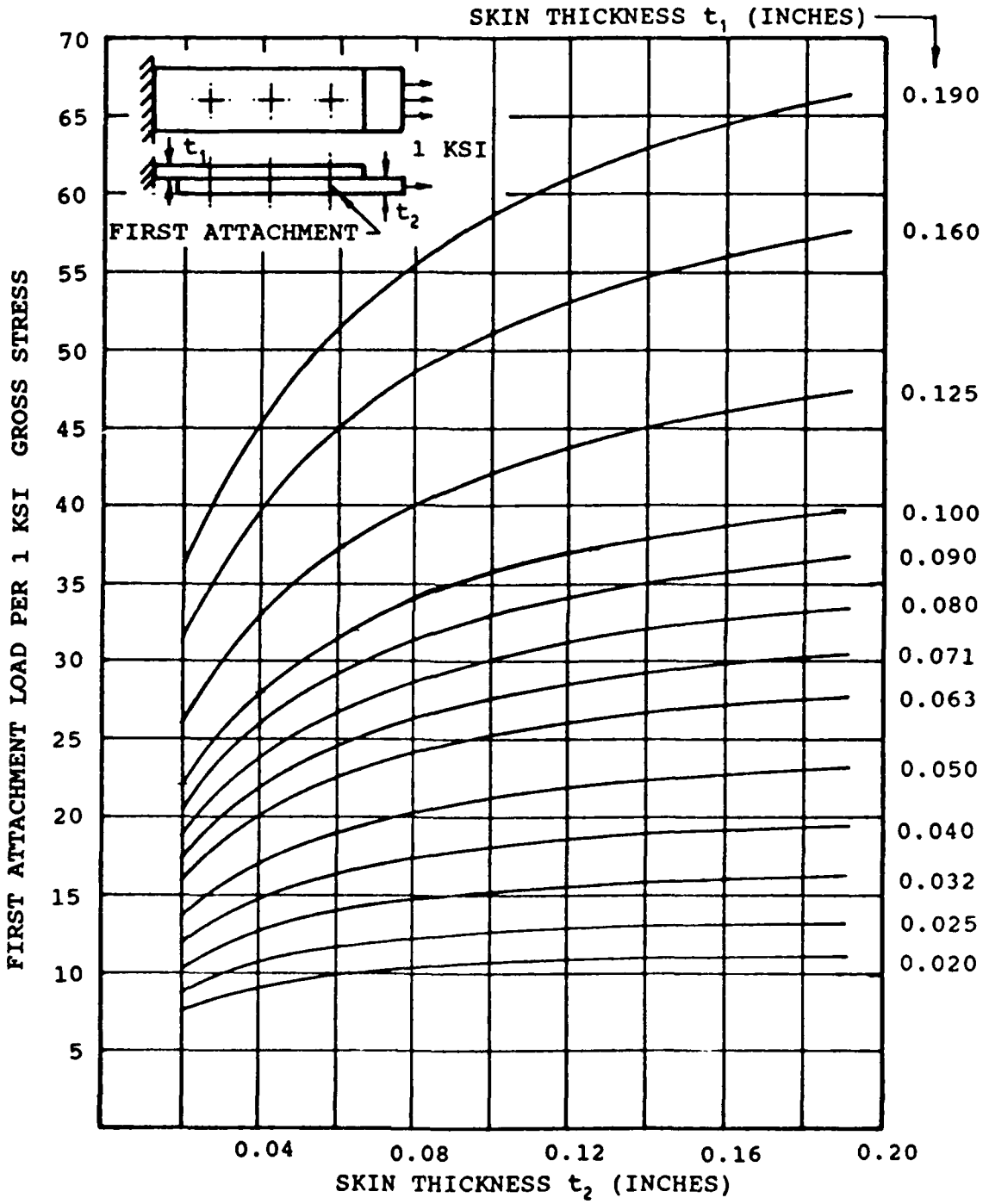

Fig. 9. First Fastener Load Per 1 KSI Gross Stress. 3 Attachment Lap Splice - 3/16 Inch Diameter Aluminum Rivets

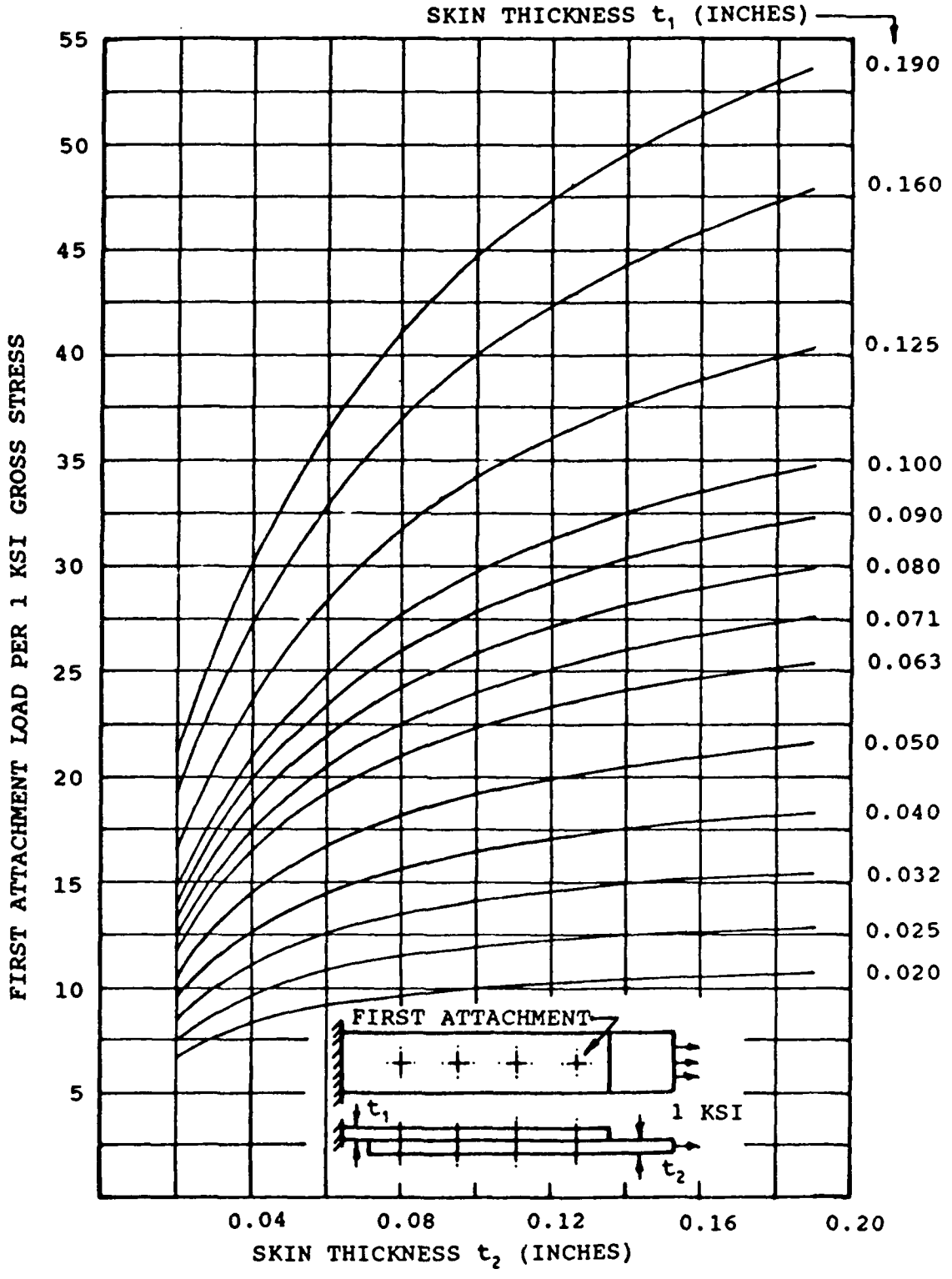

Fig. 10. First Fastener Load Per 1 KSI Gross Stress. 4 Attachment Lap Splice - 3/16 Inch Diameter Aluminum Rivets

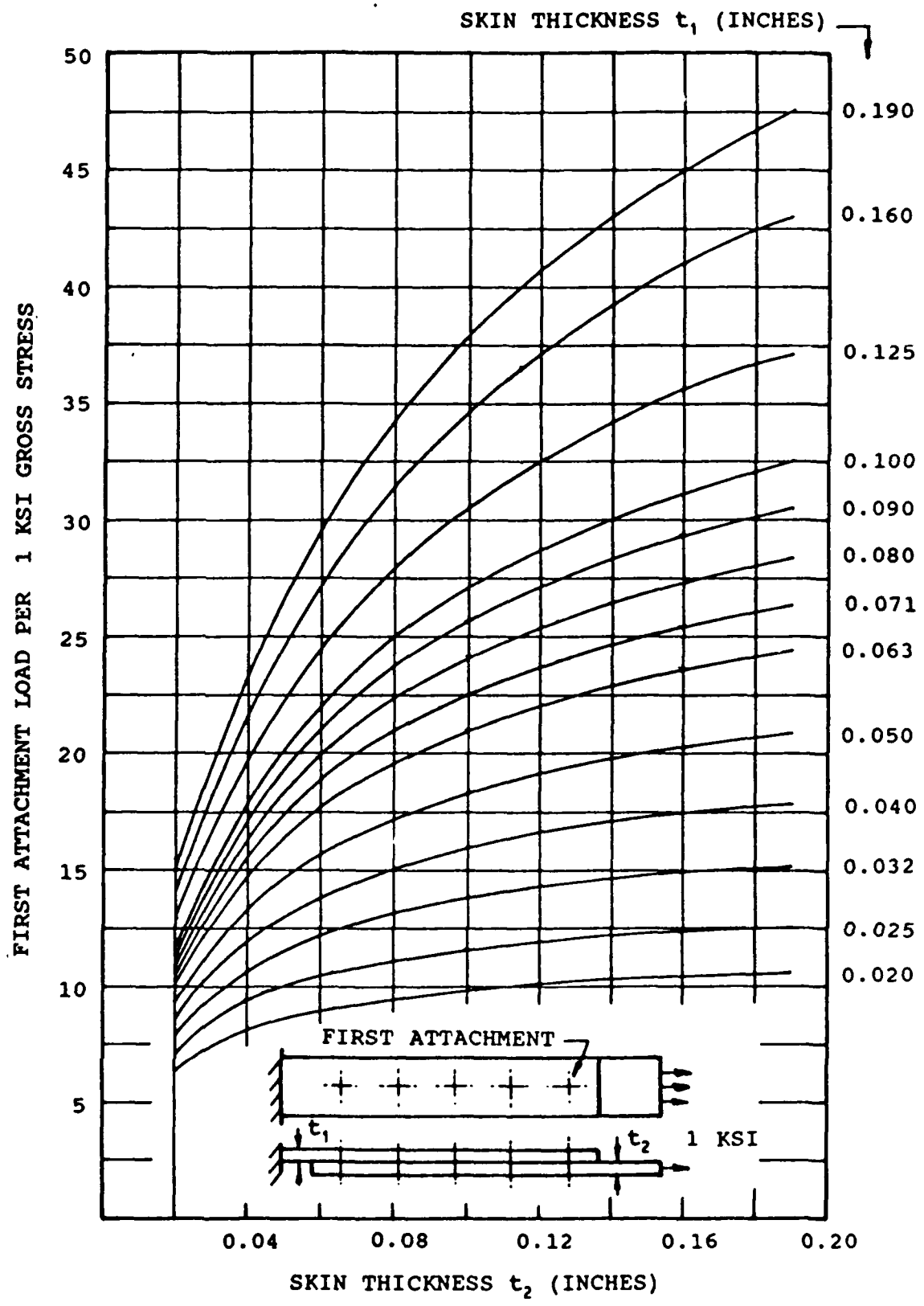

Fig. 11. First Fastener Load Per 1 KSI Gross Stress. 5 Attachment Lap Splice - 3/16 Inch Diameter Aluminum Rivets

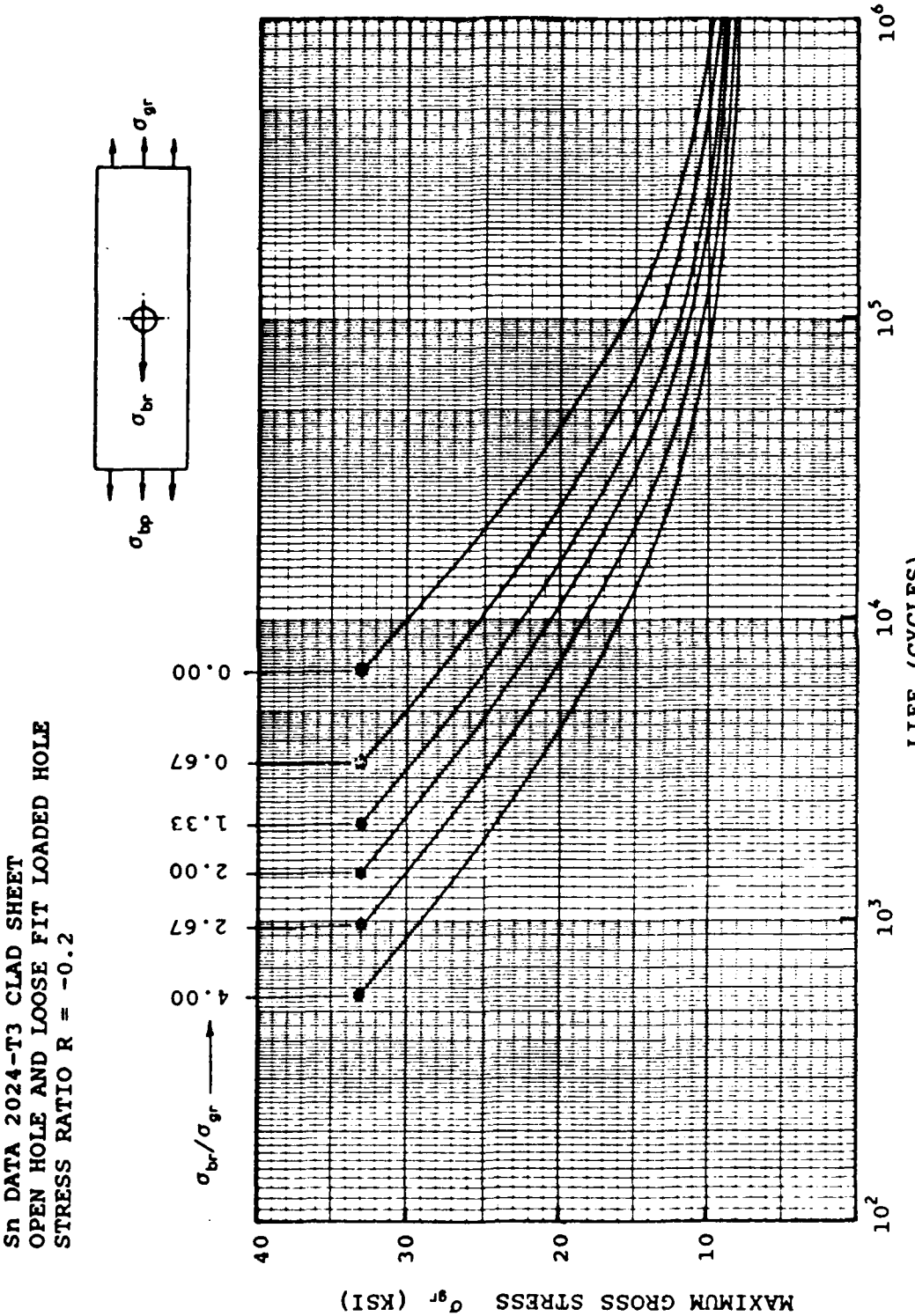

Fig. 12. Fatigue Sn Data 2024-T3, Stress Ratio R = -0.2

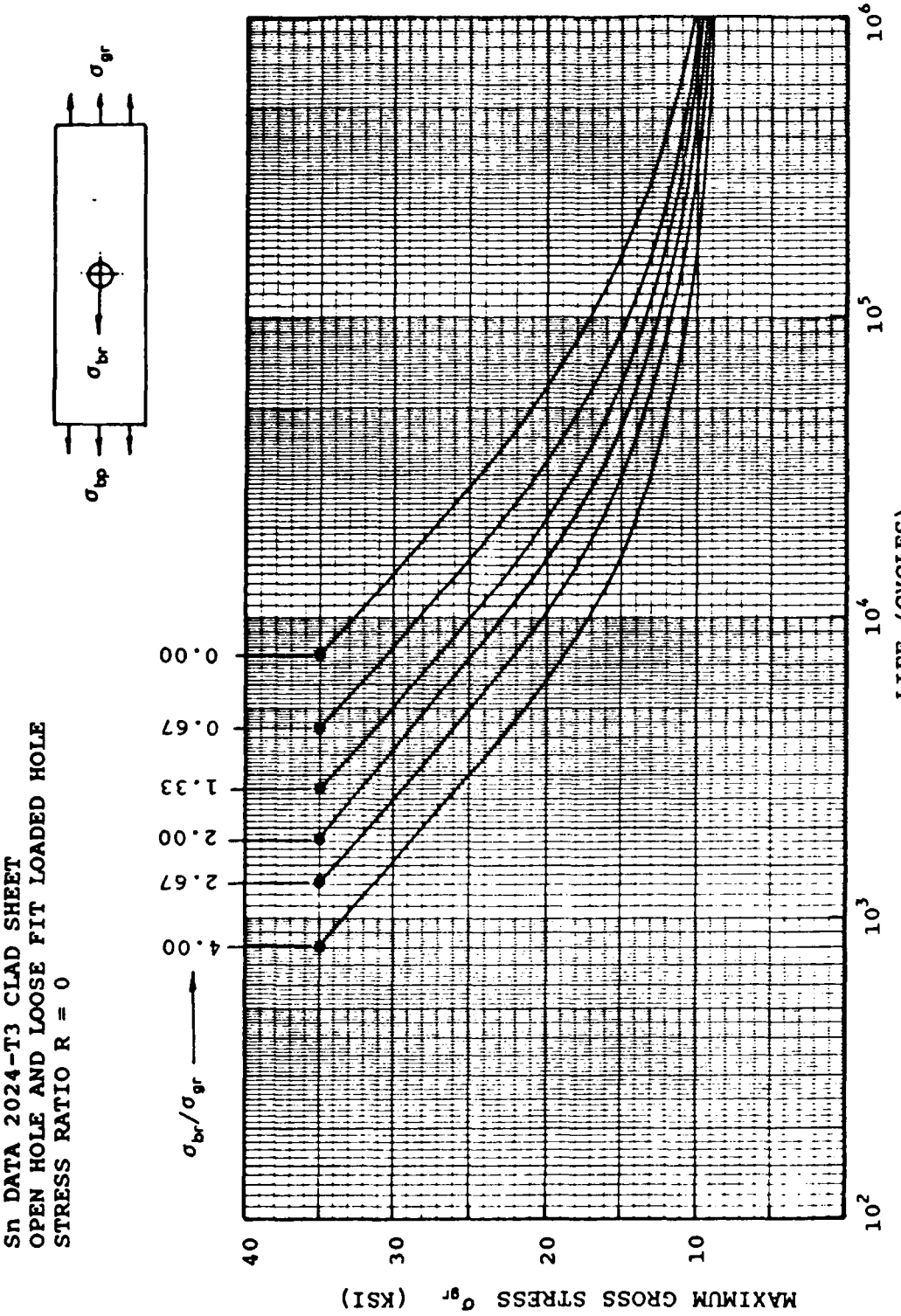

Fig. 13. Fatigue Sn Data 2024-T3, Stress Ratio R = 0.0

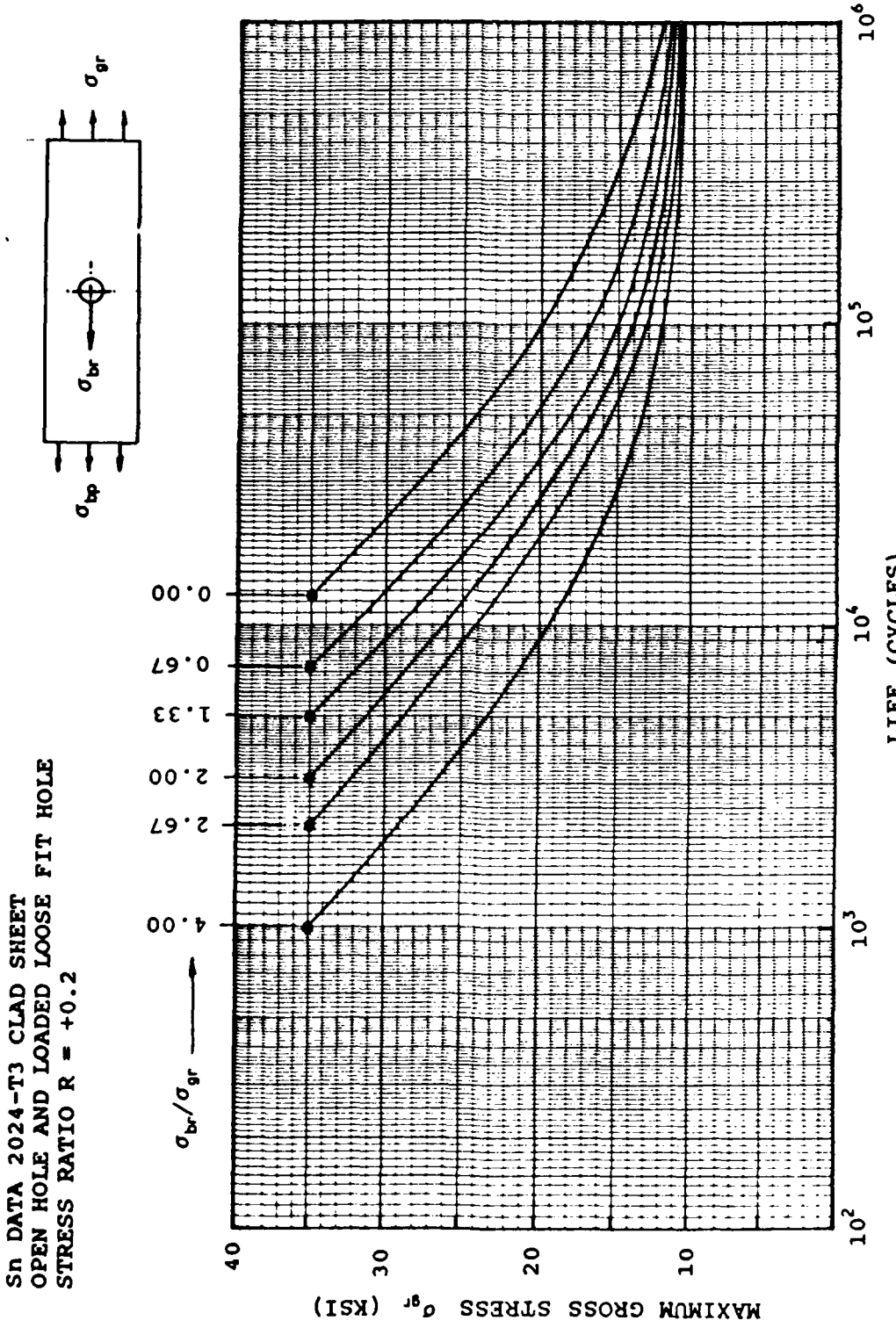

Fig. 14. Fatigue Sn Data 2024-T3, Stress Ratio R = +0.2

CYCLES REQUIRED TO GROW CRACK
FROM 0.02 INCHES TO 0.35 INCHES
AT 15.0 KSI R = 0

DOUBLER THICKNESS (INCHES)	INDUCED FASTENER LOAD (LBS)	CYCLES
0	0	27508
0.050	187.2	25524
0.063	203.4	25456
0.071	211.2	25423
0.100	232.2	25337

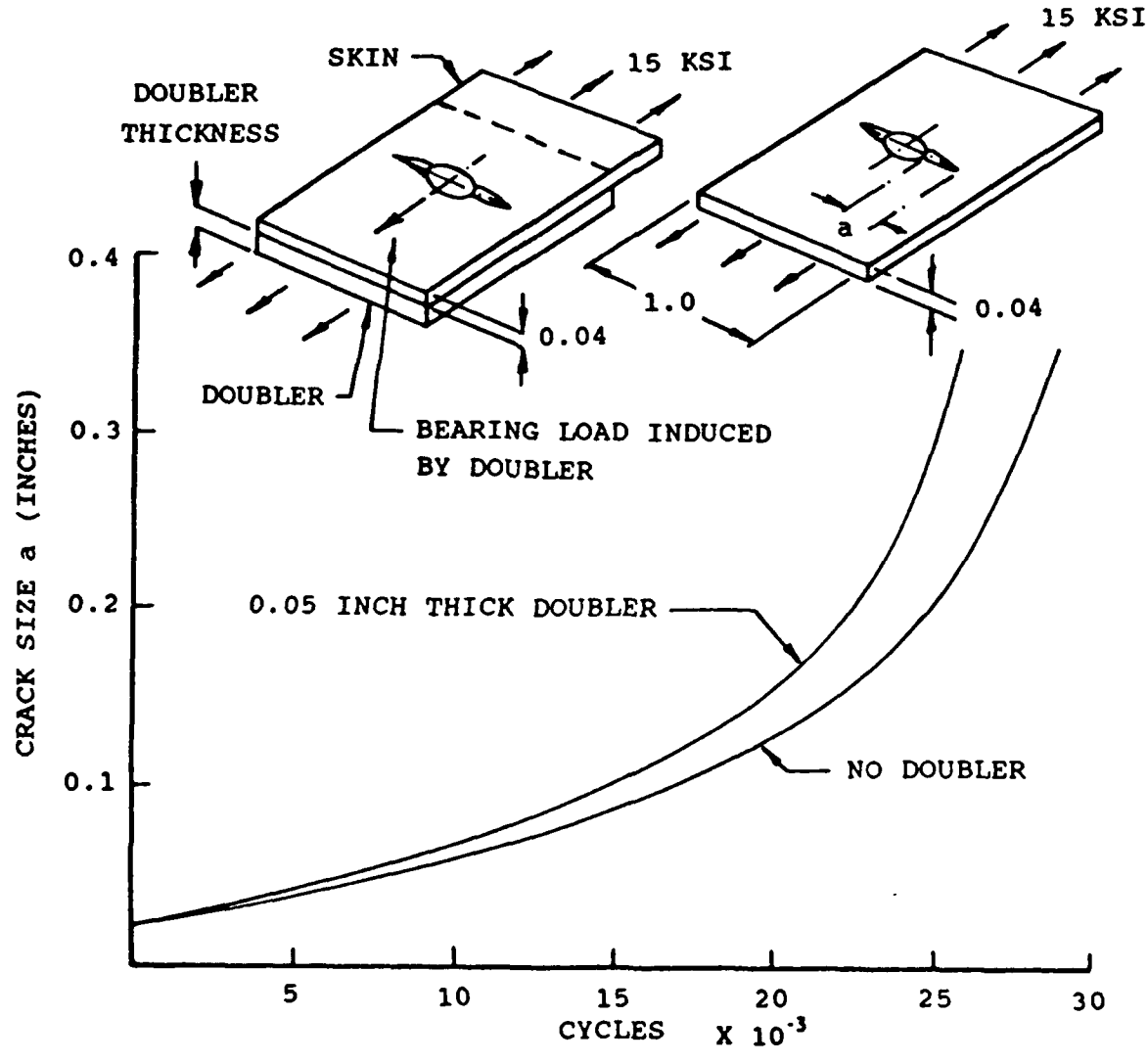

Fig. 15. Effect of Doubler Thickness on Crack Growth Life

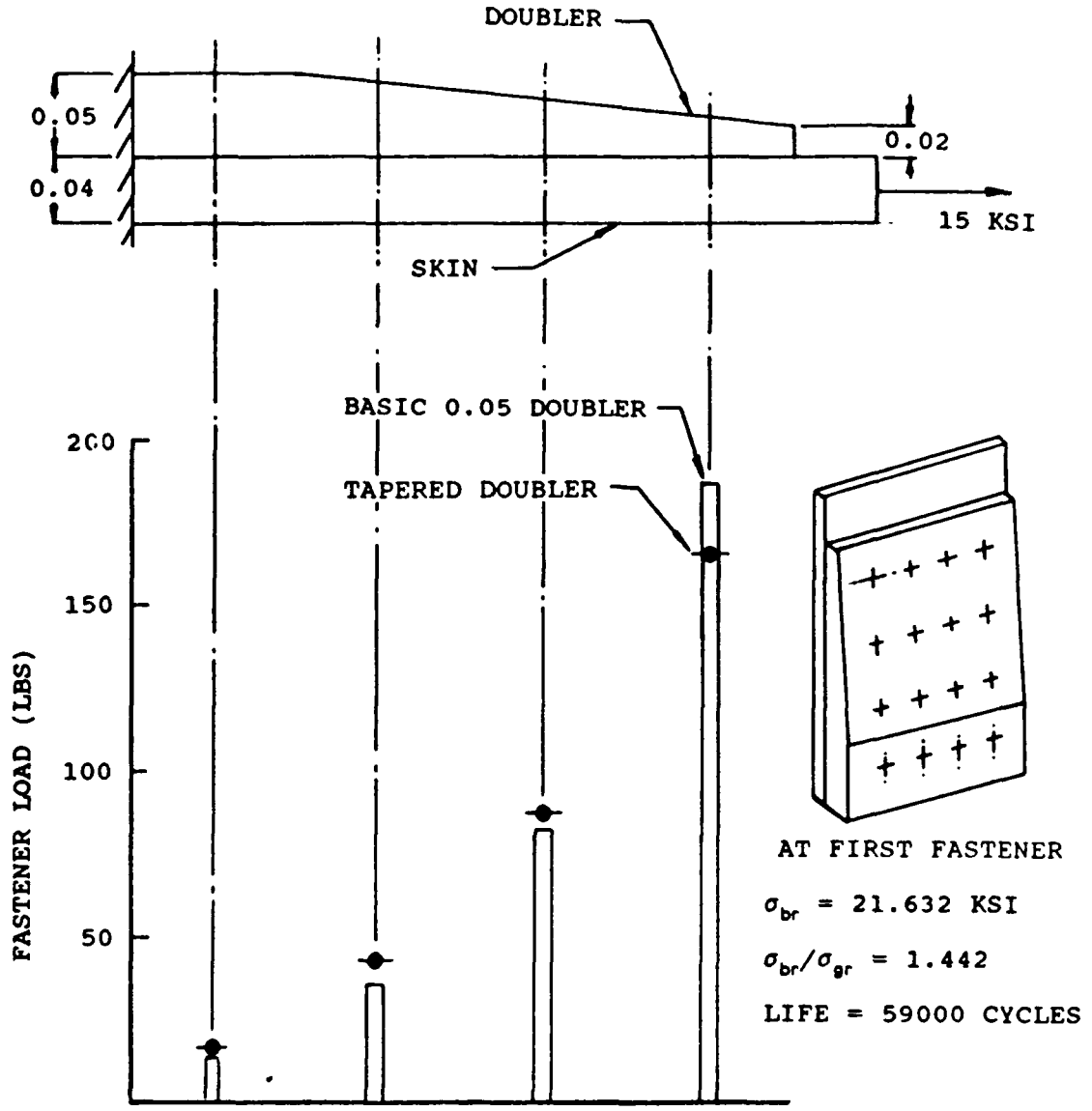

Fig. 16. Effect of Doubler Tapering on First Fastener Load And Fatigue Life

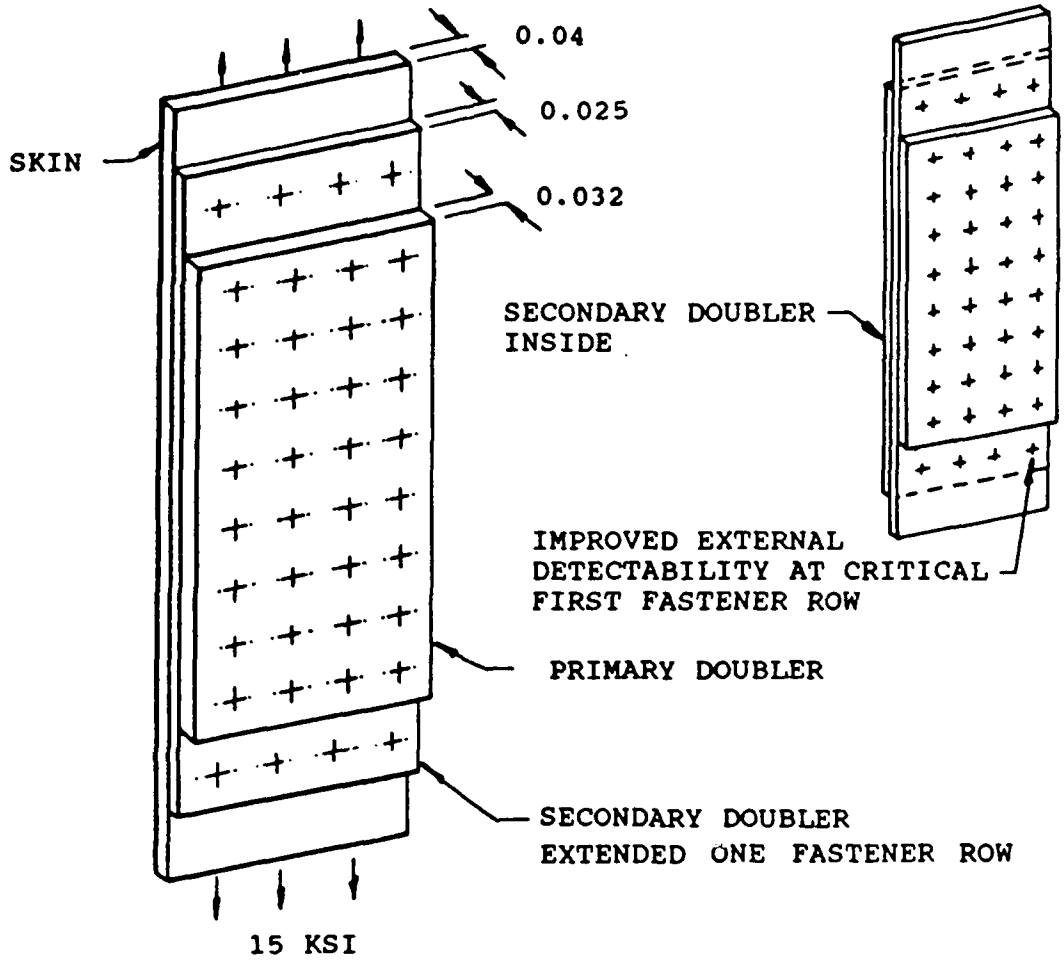

ADVANTAGES OF THIS REPAIR DESIGN

- FIRST FASTENER LOADS IN SKIN REDUCED FROM 187.2 TO 122.4 LBS
- SKIN BEARING STRESS σ_{br} REDUCED FROM 24.632 KSI TO 16.105 KSI
- BEARING STRESS TO GROSS STRESS RATIO σ_{br}/σ_{gr} REDUCED FROM 1.642 TO 1.074
- FATIGUE LIFE INCREASED FROM 53,800 CYCLES TO 70,500 CYCLES

Fig. 17. Improved Fatigue Life by Doubler Lamination

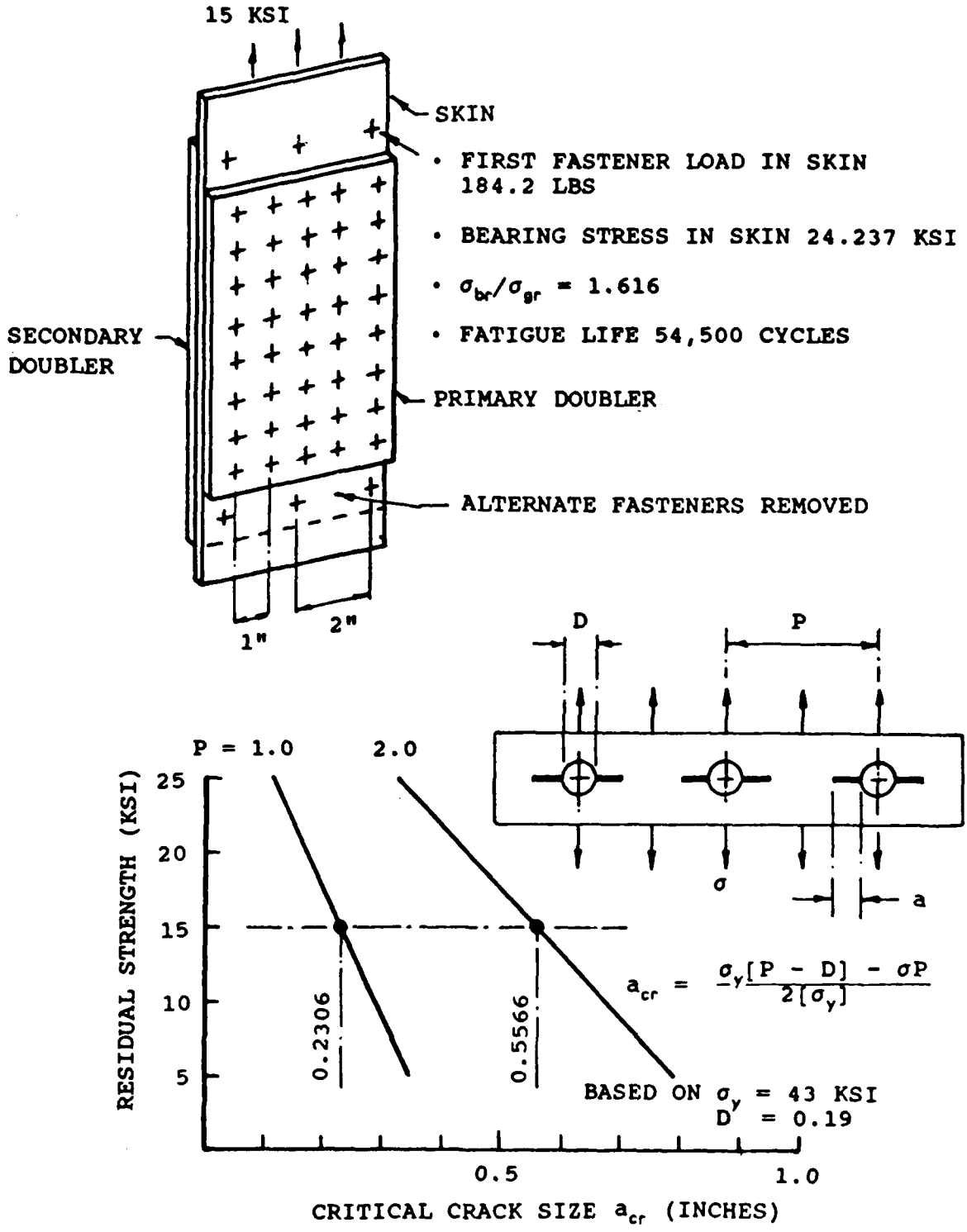

Fig. 18. Improved Crack Detectability By Removing Alternate Fasteners In Critical Row

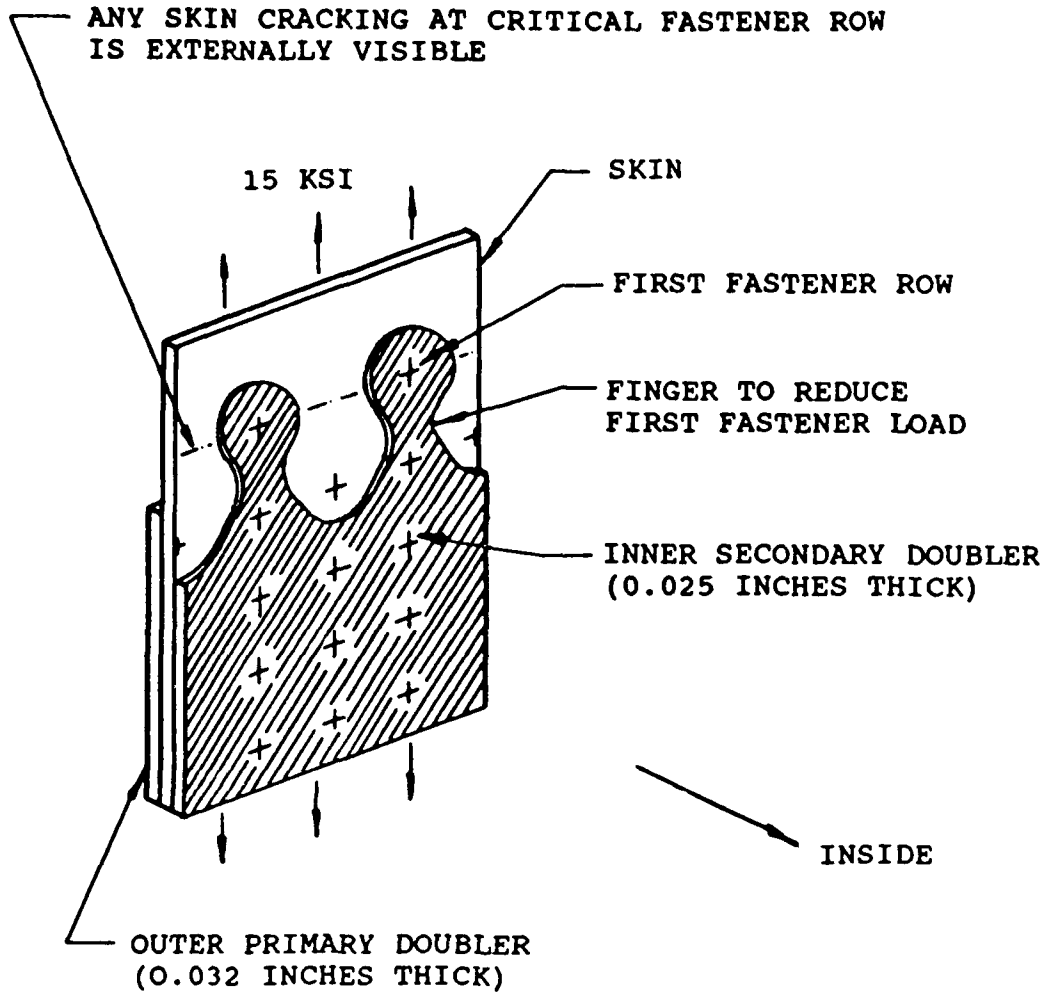

- FIRST FASTENER LOAD IN SKIN 174 LBS
- BEARING STRESS IN SKIN 22.895 KSI
- σ_{br}/σ_{gr} = 1.526
- FATIGUE LIFE 57,000 CYCLES

Fig. 19. Finger Doubler Configuration To Reduce First Fastener Load, Improve Fatigue Initiation Life And Skin Crack Detectability

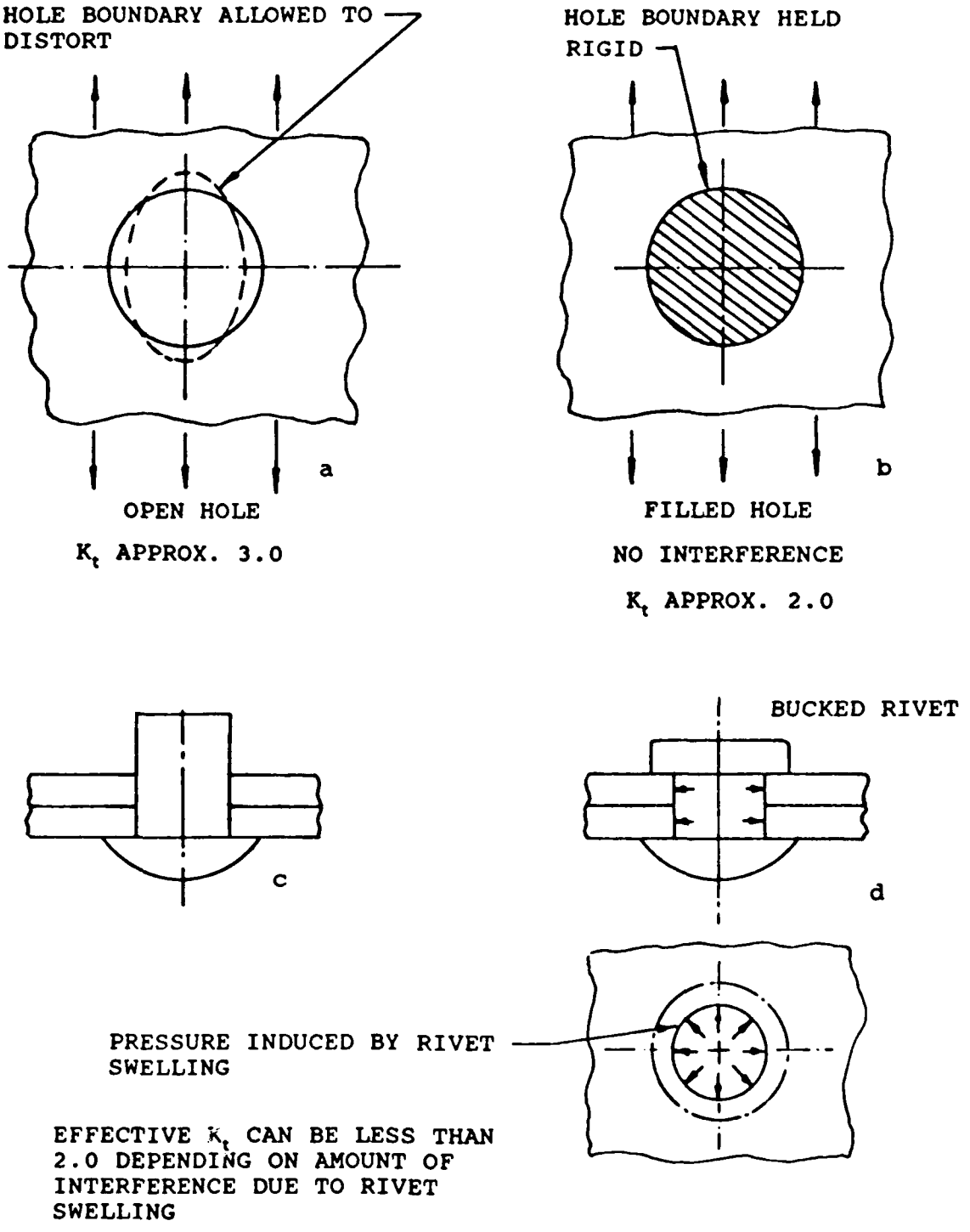

Fig. 20. Effect Of Riveting On Stress Concentration Factor

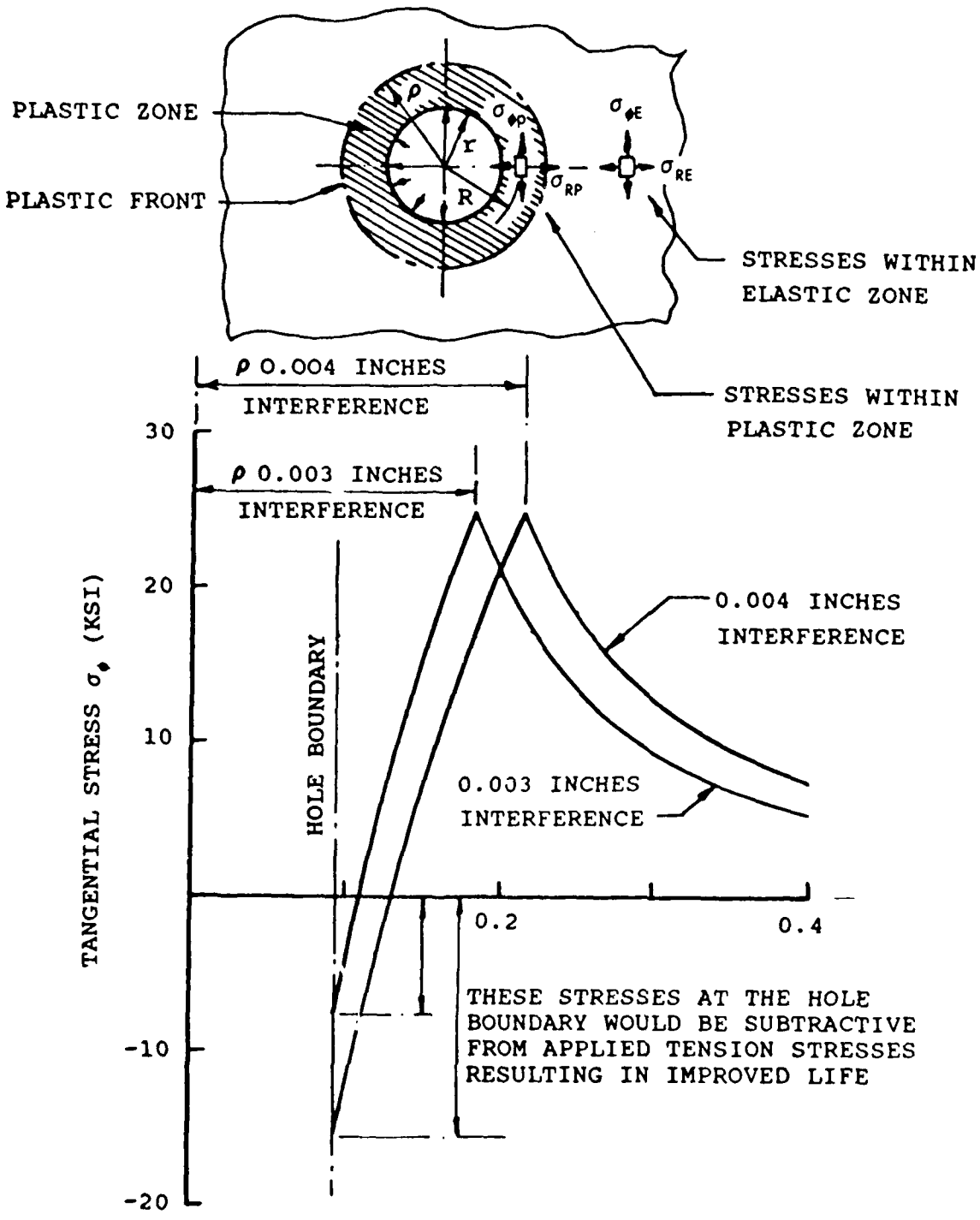

Fig. 21. Elastic-Plastic Stress Distribution Around a 0.19 Inch Diameter Rivet In 2024-T3 Sheet With Varying Degrees Of Equivalent Interference

EXAMPLE OF RIVET CLINCHING
FROM AN ACTUAL FIELD REPAIR

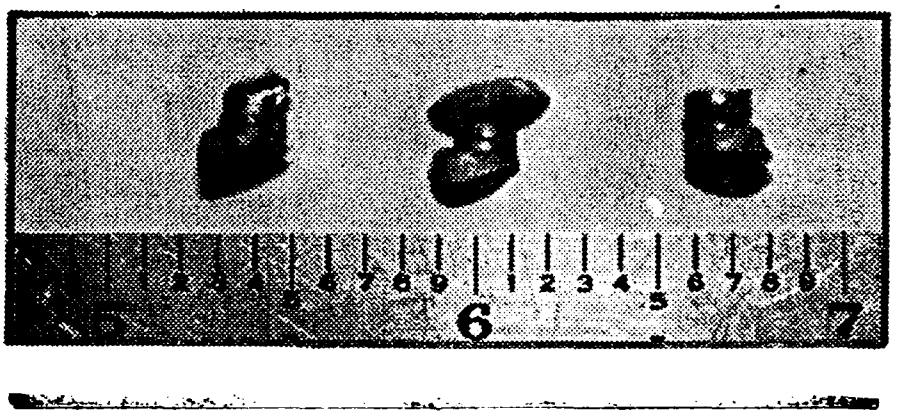

RIVETS REMOVED FROM THE
REPAIR

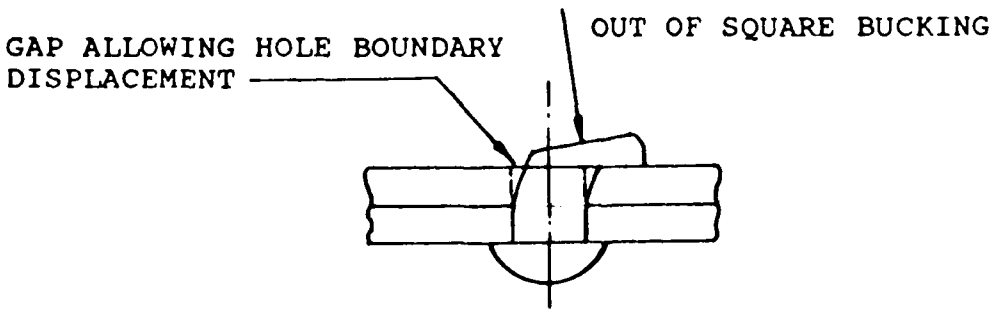

Fig. 22. Examples Of Rivet Clinching

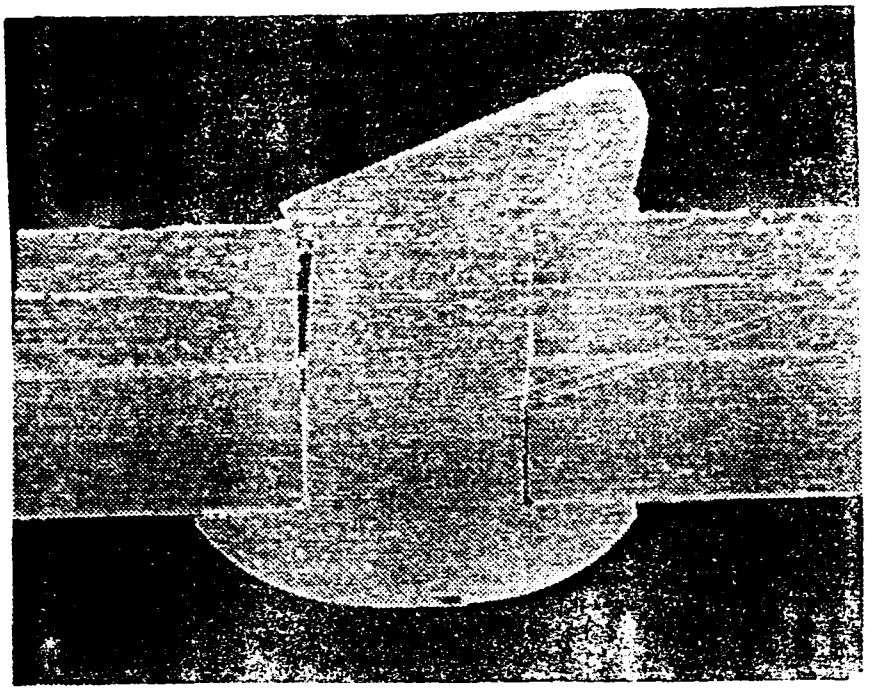

Fig. 23. Lack Of Rivet Hole Filling Due To Clinching

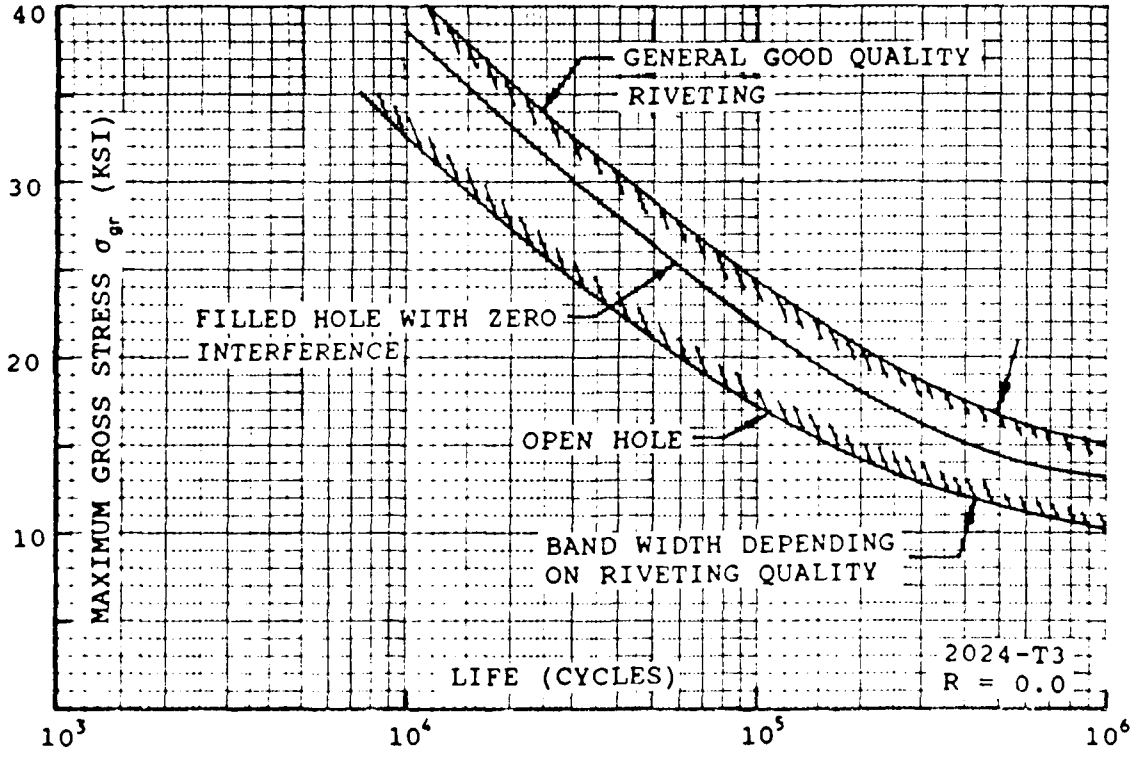

Fig. 24. Effect Of Riveting Quality On Fatigue Life

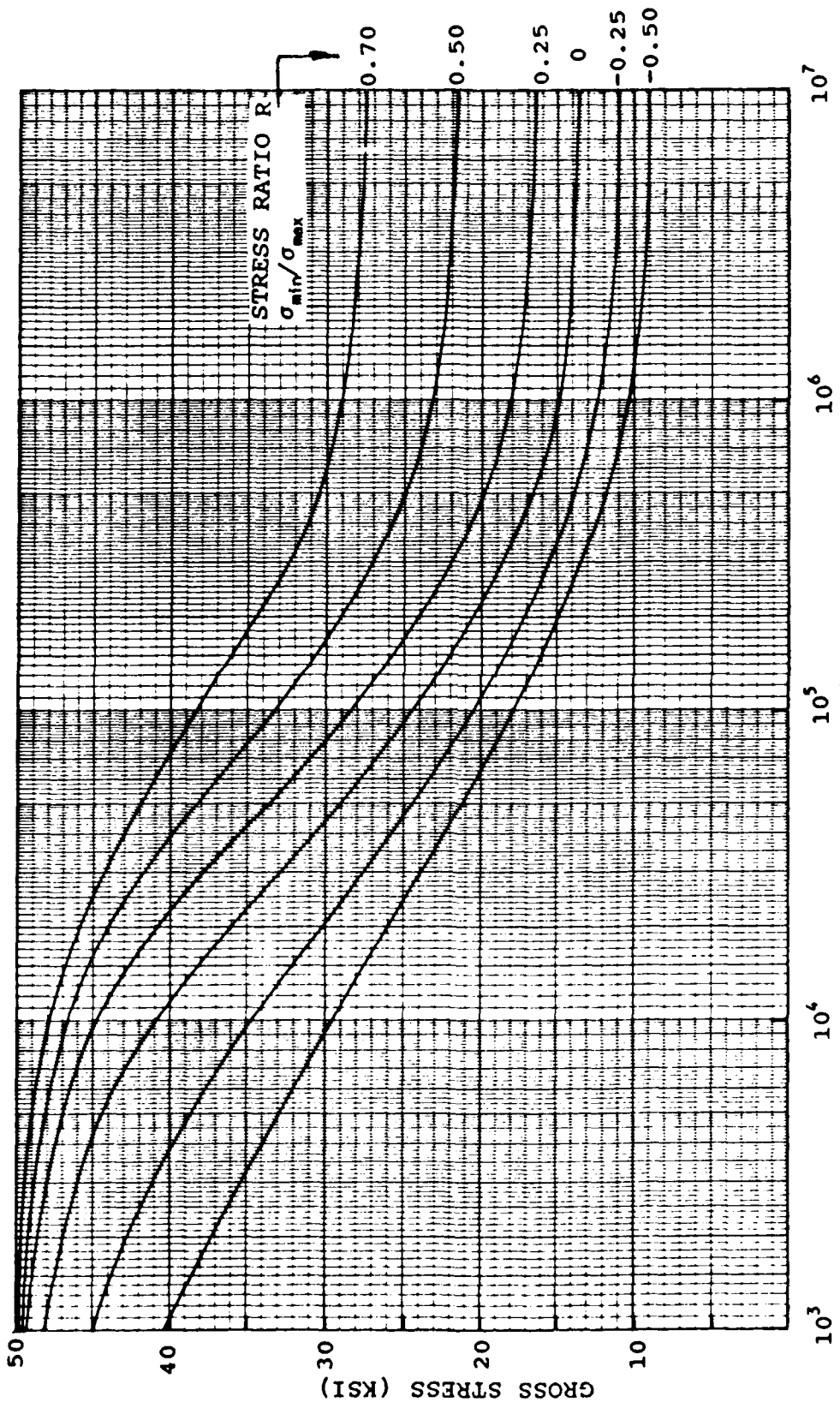

Fig. 25. Fatigue Sn Data For Good Quality 3/16 Inch Diameter Rivets In 2024-T3 Material

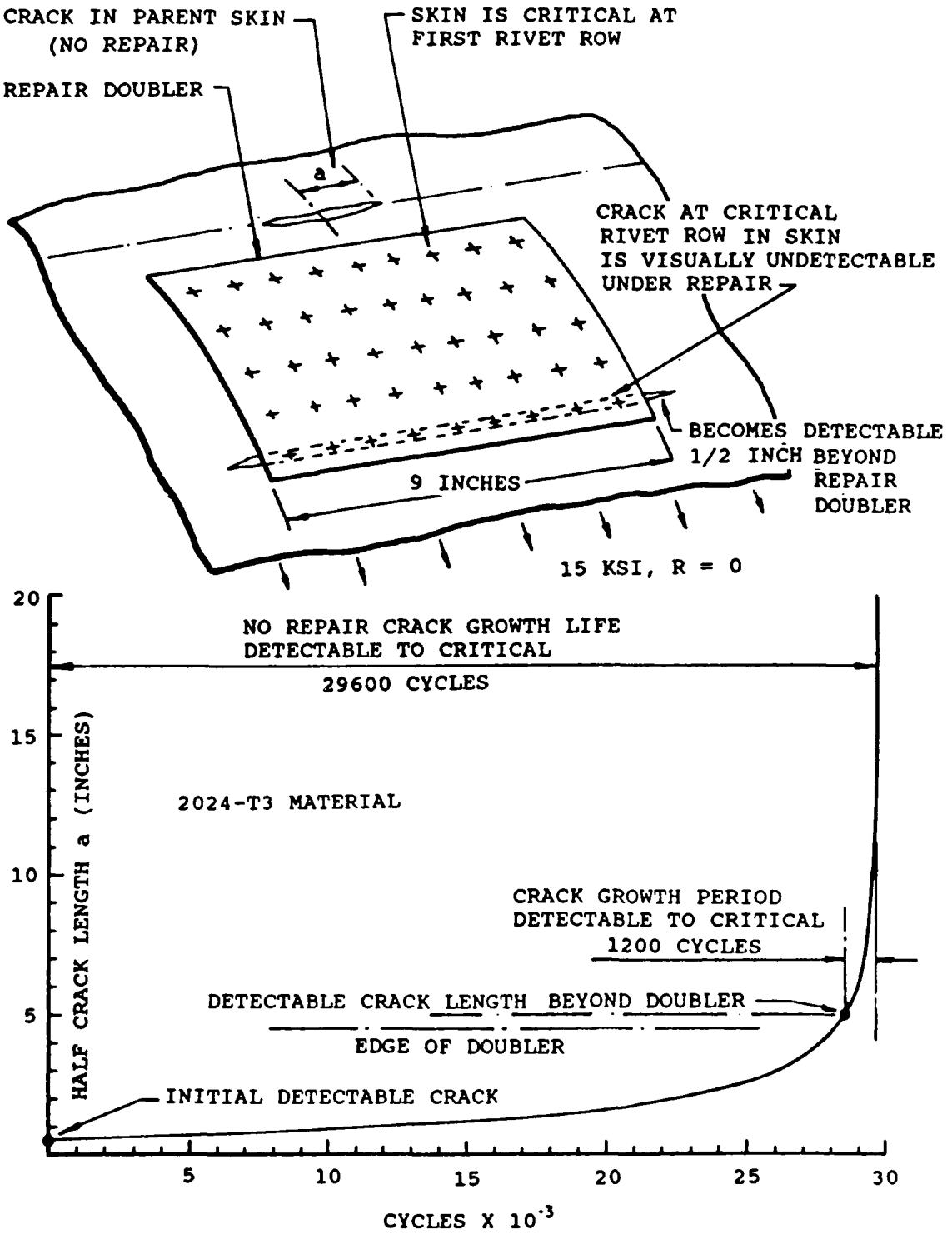

Fig. 26. Example Of Impaired Crack Growth Detectability With Repair Doubler

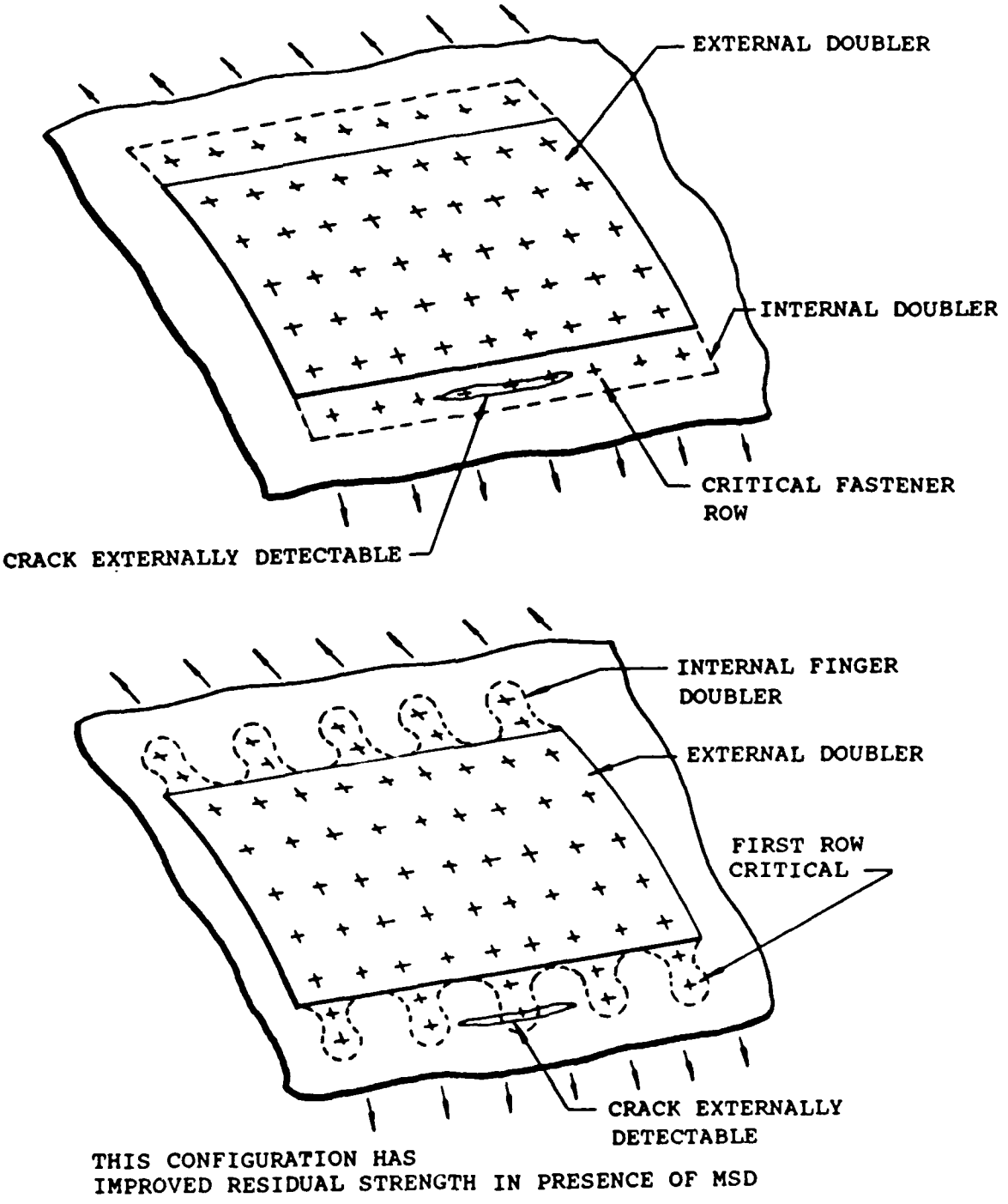

Fig. 27. Improved Doubler Design For External Detectability And Residual Strength Improvement

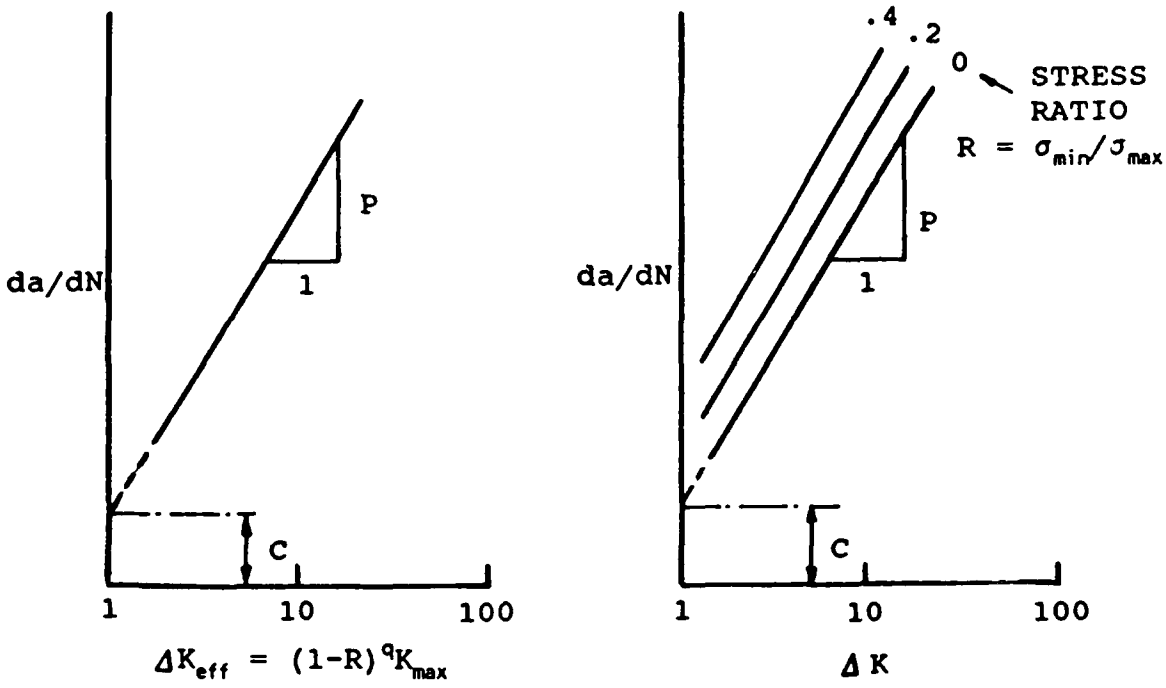

$$da/dN = C\{(1-R)^q K_{max}\}^p$$

where C = Intercept with K = 1.0 ordinate

R = Stress Ratio $\sigma_{min}/\sigma_{max}$

q = Exponent to control width of R ratio band of lines

K_{max} = Maximum stress intensity factor $\sigma_{max}\sqrt{\pi a}$

σ_{max} = Maximum applied gross stress

β = Geometry effect

P = Slope of da/dN line

Fig. 28. Walker Crack Growth Rate Equation

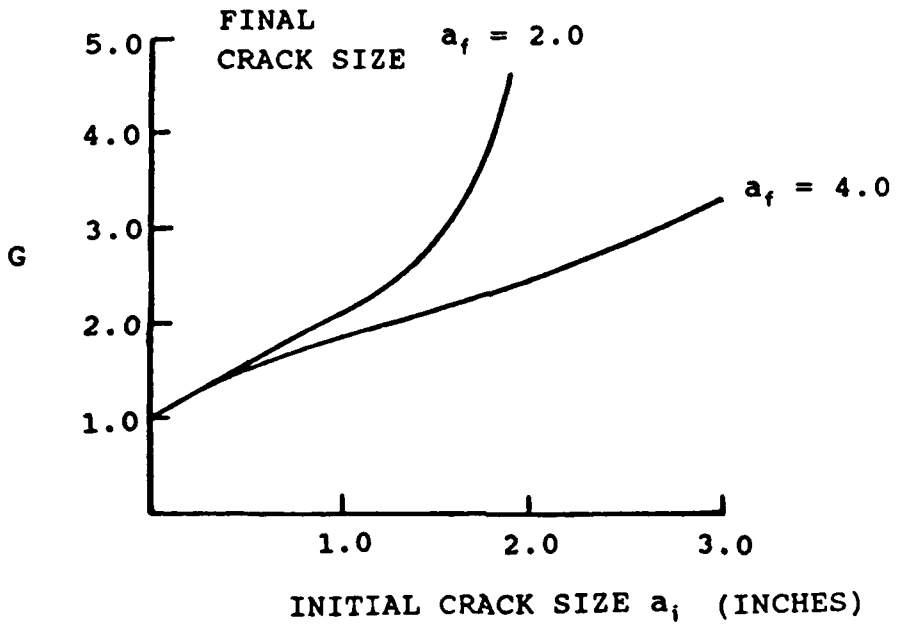

Fig. 29. Example Of The Geometric Term G For An Infinitely Wide Panel

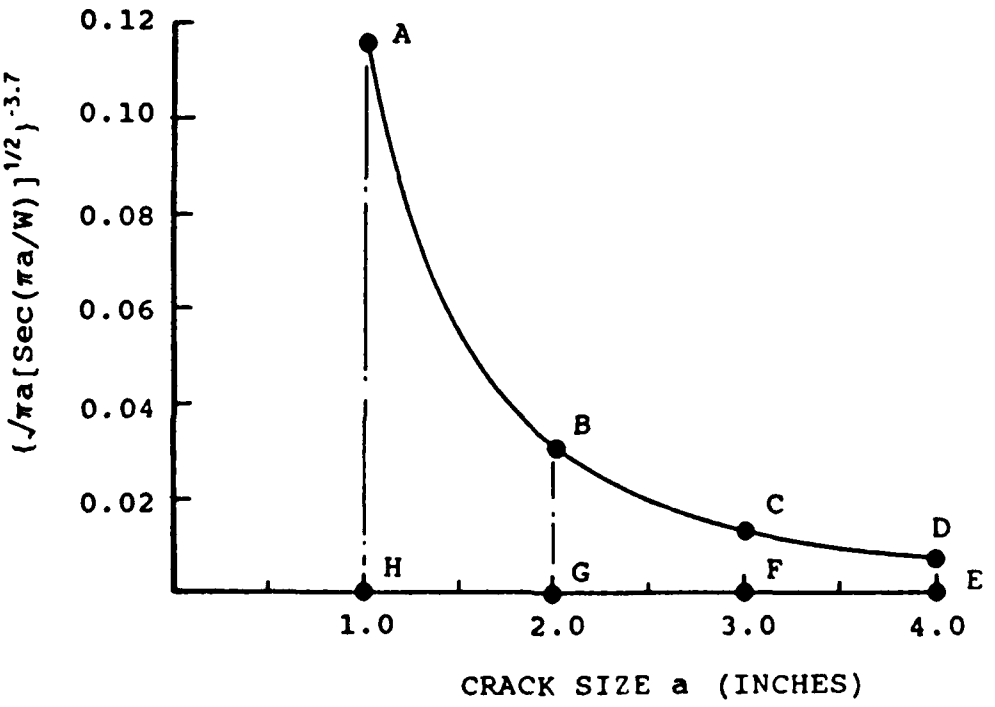

Fig. 30. Curve Of $(\sqrt{\pi a}\,\beta)^{-P}$ For Finite Width Panel

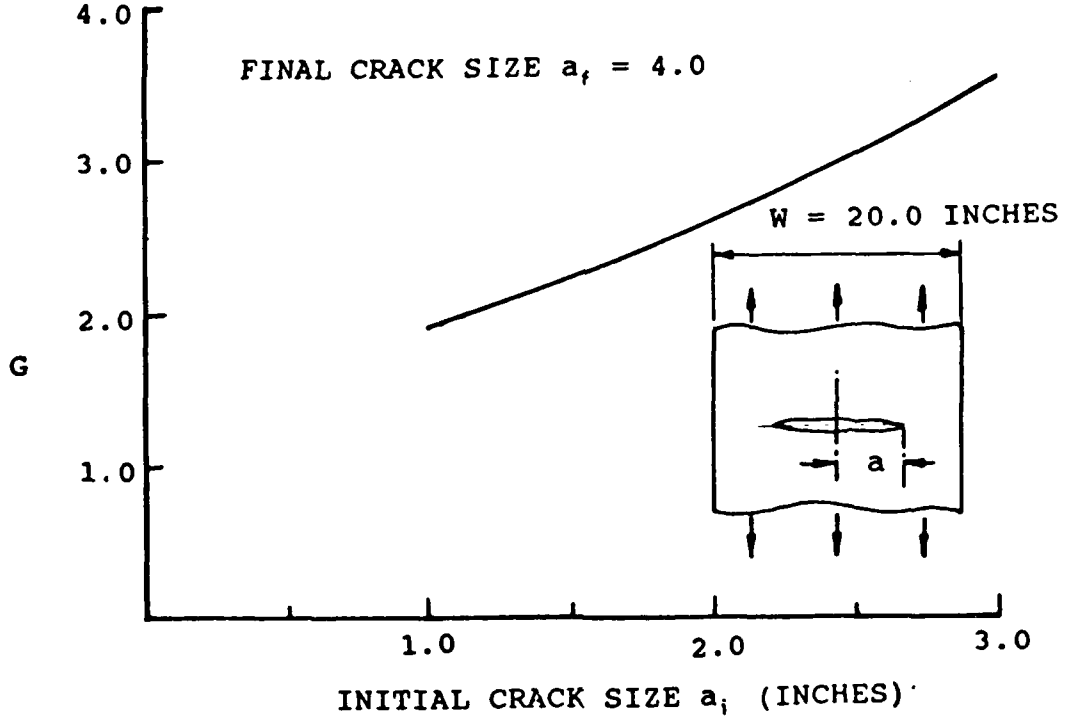

Fig. 31. Example Plot Of G For 20.0 Inch Wide Panel

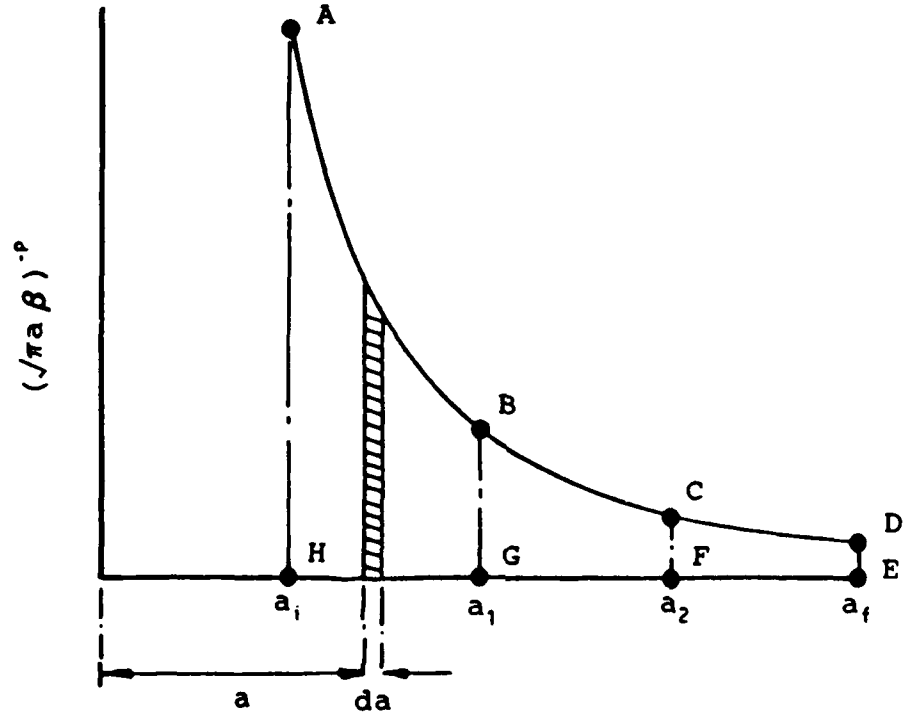

Fig. 32. Step Integration of $(\sqrt{\pi a}\,\beta)^{-p}$

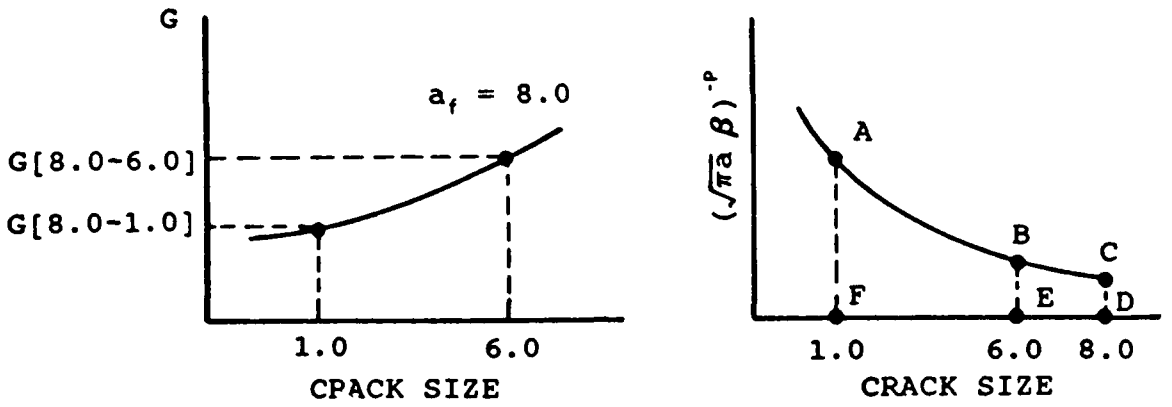

Fig. 33. Integration of G^{-P} In Pieces

$$G[2.0\text{-}1.0] = \{[G(8.0\text{-}1.0)]^{-P} - [G(8.0\text{-}2.0)]^{-P}\}^{-1/P}$$

$$G[3.0\text{-}1.0] = \{[G(8.0\text{-}1.0)]^{-P} - [G(8.0\text{-}3.0)]^{-P}\}^{-1/P}$$

$$G[4.0\text{-}1.0] = \{[G(8.0\text{-}1.0)]^{-P} - [G(8.0\text{-}4.0)]^{-P}\}^{-1/P}$$

$$G[5.0\text{-}1.0] = \{[G(8.0\text{-}1.0)]^{-P} - [G(8.0\text{-}5.0)]^{-P}\}^{-1/P}$$

$$N_1 = N[2.0\text{-}1.0] = 1/C\{[G(2.0\text{-}1.0)]S\}^{-P}$$

$$N_2 = N[3.0\text{-}1.0] = 1/C\{[G(3.0\text{-}1.0)]S\}^{-P}$$

$$N_3 = N[4.0\text{-}1.0] = 1/C\{[G(4.0\text{-}1.0)]S\}^{-P}$$

$$N_4 = N[5.0\text{-}1.0] = 1/C\{[G(5.0\text{-}1.0)]S\}^{-P}$$

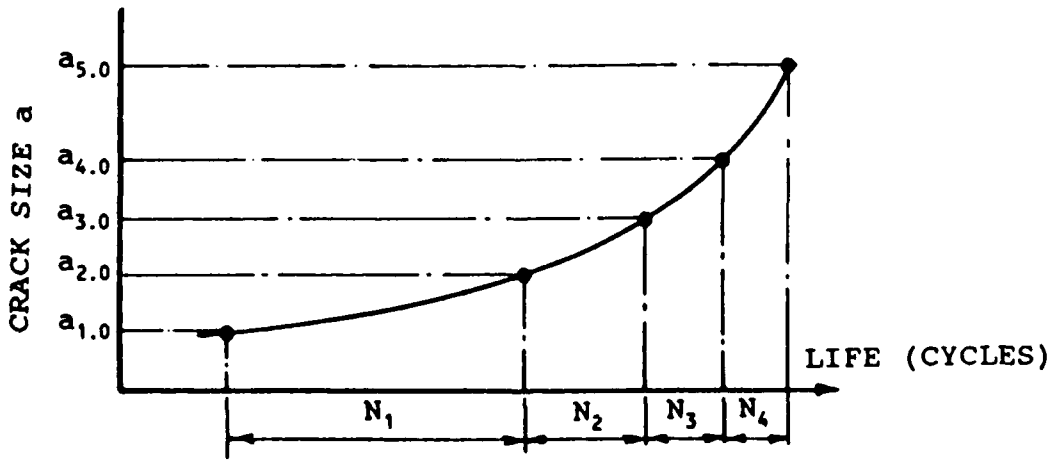

Fig. 34. G For Various Points On Crack Growth Curve

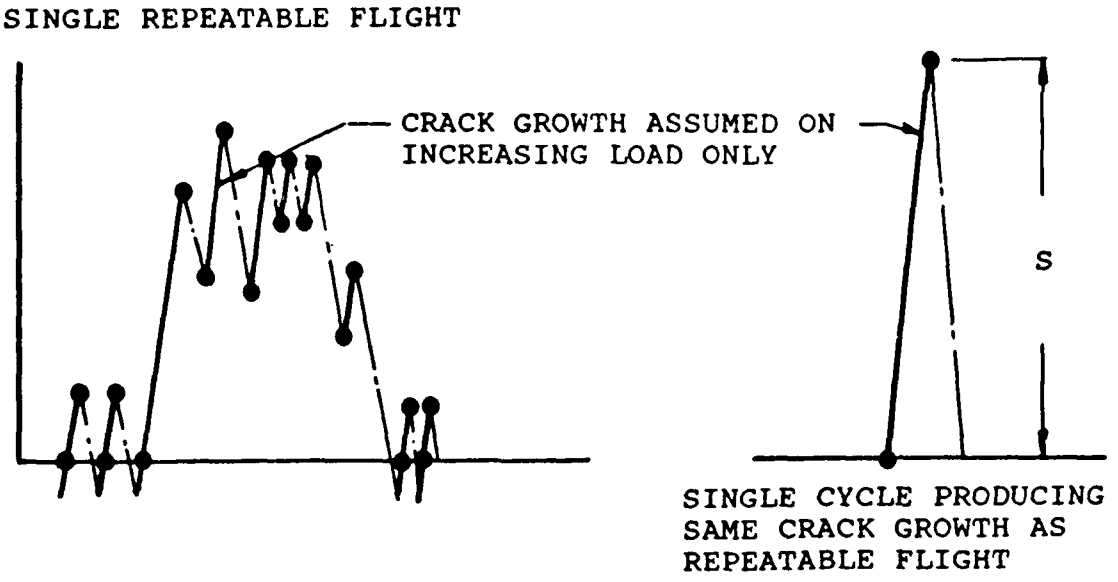

Fig. 35. Simulation Of Repeatable Flight To A Single Cycle

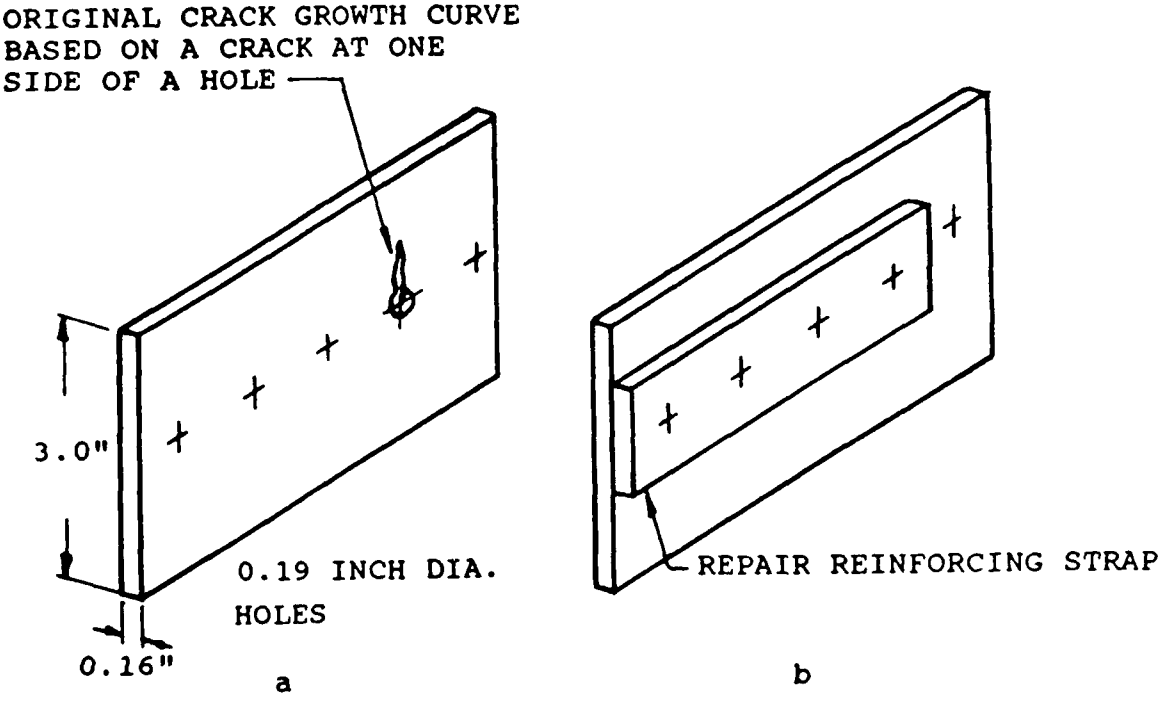

Fig. 36. Example Of Repaired Element

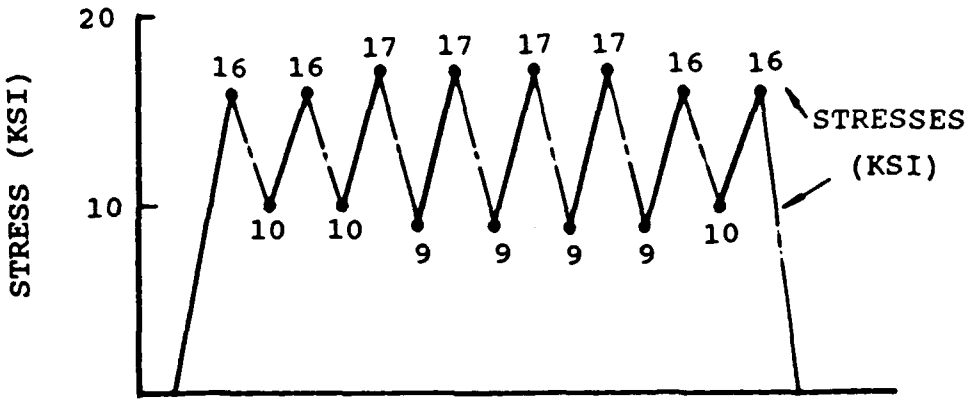

Fig. 37. Simple Example Spectrum For Repeatable Flight

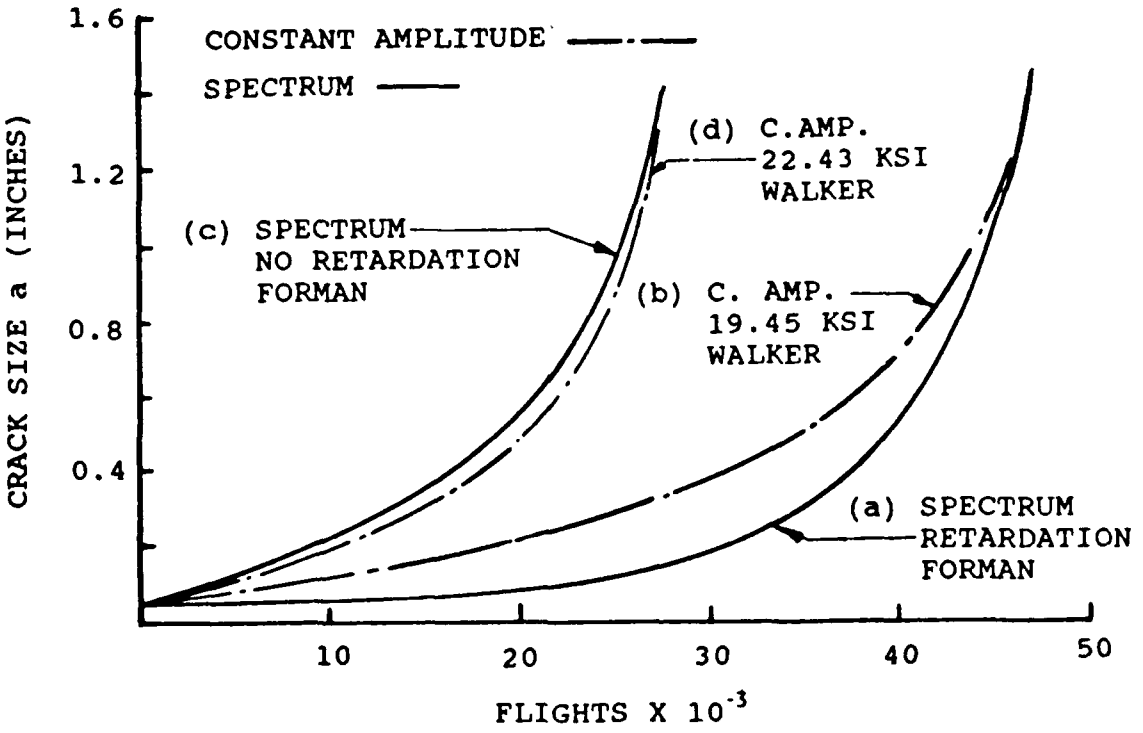

Fig. 38 Crack Growth Comparison Spectrum/Constant Amplitude

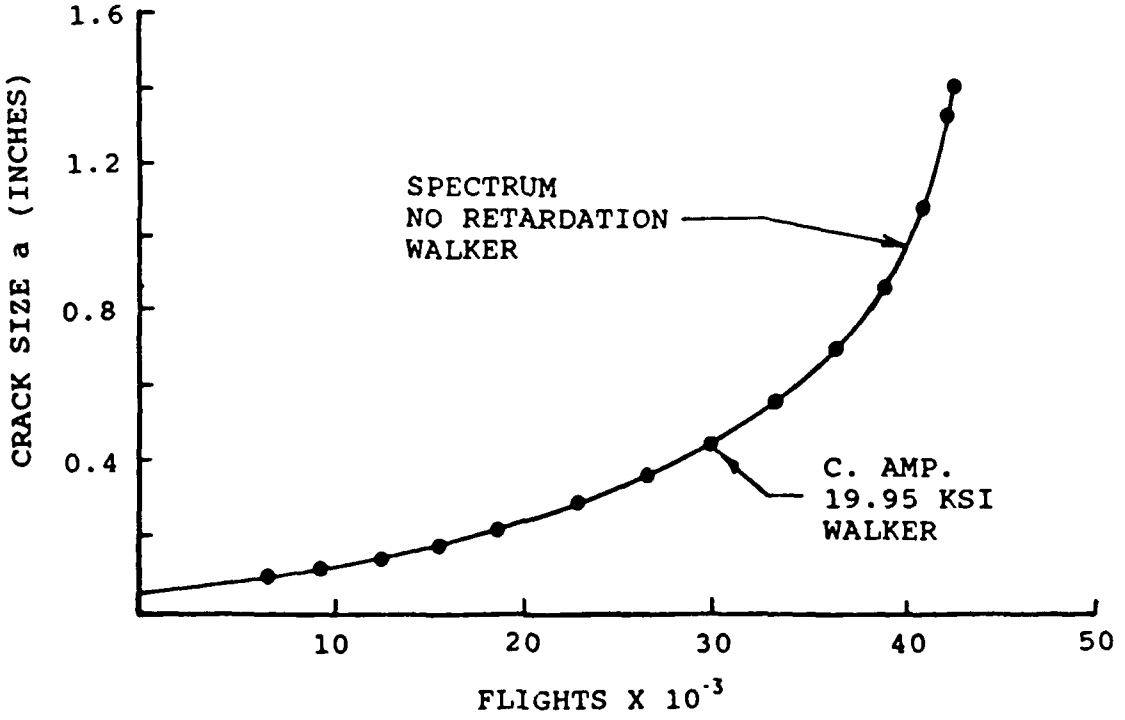

Fig. 39. Crack Growth Comparison Spectrum/Constant Amplitude Using Same Crack Growth Equation